LETTERS
https://doi.org/10.1038/s41591-019-0563-7
nature medicine

Contribution of genetics to visceral adiposity and its relation to cardiovascular and metabolic disease

Torgny Karlsson*, Mathias Rask-Andersen, Gang Pan, Julia Höglund, Claes Wadelius, Weronica E. Ek and Åsa Johansson*

Visceral adipose tissue (VAT)—fat stored around the internal organs—has been suggested as an independent risk factor for cardiovascular and metabolic disease[1–3], as well as all-cause, cardiovascular-specific and cancer-specific mortality[4,5]. Yet, the contribution of genetics to VAT, as well as its disease-related effects, are largely unexplored due to the requirement for advanced imaging technologies to accurately measure VAT. Here, we develop sex-stratified, nonlinear prediction models (coefficient of determination = 0.76; typical 95% confidence interval (CI) = 0.74–0.78) for VAT mass using the UK Biobank cohort. We performed a genome-wide association study for predicted VAT mass and identified 102 novel visceral adiposity loci. Predicted VAT mass was associated with increased risk of hypertension, heart attack/angina, type 2 diabetes and hyperlipidemia, and Mendelian randomization analysis showed visceral fat to be a causal risk factor for all four diseases. In particular, a large difference in causal effect between the sexes was found for type 2 diabetes, with an odds ratio of 7.34 (95% CI = 4.48–12.0) in females and an odds ratio of 2.50 (95% CI = 1.98–3.14) in males. Our findings bolster the role of visceral adiposity as a potentially independent risk factor, in particular for type 2 diabetes in Caucasian females. Independent validation in other cohorts is necessary to determine whether the findings can translate to other ethnicities, or outside the UK.

The global prevalence of obesity and overweight has risen dramatically over the past century[6], and the conditions constitute a severely increasing health problem worldwide. Visceral fat has been shown to be more harmful compared with fat stored elsewhere in the body[1,2]. Visceral adipose tissue (VAT) mass can be estimated accurately by magnetic resonance imaging, computed tomography or dual-energy X-ray absorptiometry (DXA). Unfortunately, these are all costly and time-consuming techniques that require substantial infrastructure investments, as well as specialized medical staff. To this end, we developed novel, nonlinear prediction models from associated variables that are more easily measured than VAT itself. The models were calibrated using a large training dataset, with VAT measured by DXA in 4,198 individuals (Extended Data Fig. 1) of white British ancestry from the UK Biobank (UKBB).

Measured VAT mass was regressed on an extensive number of demographic, anthropometric and bioelectrical impedance predictors of the arms, legs and whole body (Supplementary Tables 1 and 2 and Extended Data Fig. 2). Two reduced prediction models, which included only nominally significant regression terms, were developed for use in the clinic, while the two full models included all terms (Supplementary Table 3). These models were adopted to predict the VAT mass in nearly 400,000 white British participants of the UKBB, of which 325,153 were used in the downstream analyses (Extended Data Fig. 1). Overall, the training and application datasets had similar characteristics and the median depot of VAT was ~2.5 times larger in males compared with females (Supplementary Table 2). The coefficients of determination (R^2), as well as the adjusted coefficients of determination, were estimated to $R^2 = 0.76$ for all prediction models, with a 95% confidence interval (CI) of 0.74–0.78 for the majority of models (Supplementary Table 4). All models showed a highly significant improvement ($P < 0.0001$), higher R^2 and higher predicted R^2 over those models that only included linear terms and no bioelectrical impedance predictors (Supplementary Table 5a,b). The models were not overfitted, as was evident by the consistently high predicted R^2 values and the out-of-sample validation (Supplementary Tables 4 and 6a,b, Extended Data Figs. 3 and 4, and see also Supplementary Text). Several earlier attempts[7–10] have been made to predict VAT using multiple linear regression modeling. Of these, the two largest studies ($n = 350–600$) with the most accurate estimates of the coefficient of determination have reported an $R^2 \leq 0.69$ (refs. [8,9]). We argue that higher-order terms, such as interactions, should be a natural component of VAT prediction models that are based on anthropometric measures (Supplementary Text), and conclude that the increase in explained variance, compared with earlier linear prediction models[8,9], is predominantly due to the adoption of a more complex model (Supplementary Text).

Using predicted VAT mass (VAT^), we performed a large-scale genome-wide association (GWA) study (GWAS) for VAT accumulation. Up to this point, only four single-nucleotide polymorphisms (SNPs) have been identified in GWASs for VAT or VAT adjusted for body mass index (BMI)[11–13]. In the present study, we were able to identify 209 independent VAT^ associations ($P < 3.33 \times 10^{-9}$), distributed over 200 nonoverlapping loci (Supplementary Table 7). Of these, 205 signals were identified in the sex-combined analysis, while four signals were identified exclusively in the sex-specific analyses (two in females and two in males). We observed associations at several loci that have previously been associated with obesity and BMI, such as the well-studied *FTO* and *MC4R* loci. Moreover, the lead SNP rs2842895 in the *RREB1* locus, which was previously associated with VAT adjusted for BMI[13], was also nominally significant in our analysis ($P = 2.7 \times 10^{-4}$), with the same direction of effect (Supplementary Text). However, 102 of the independent loci have hitherto not been associated with any adiposity-related phenotype (Supplementary

Department of Immunology, Genetics and Pathology, Science for Life Laboratory, Uppsala University, Uppsala, Sweden. *e-mail: torgny.karlsson@igp.uu.se; asa.johansson@igp.uu.se

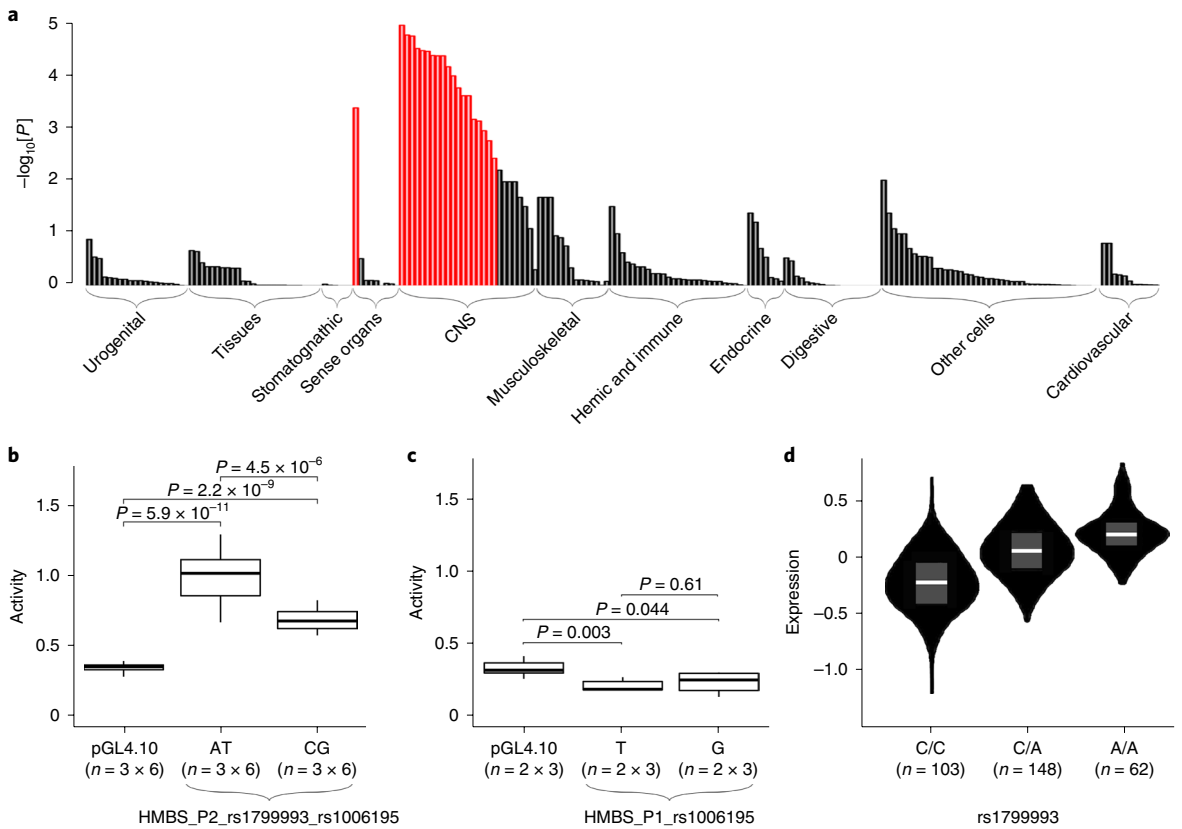

Fig. 1 | Tissue enrichment for the most significant GWA signals, and results from functional experiments for *HMBS*. **a**, Tissue enrichment results from DEPICT. Tissues are grouped together based on similarities or on the organ from which the tissues were derived. Each bar represents one tissue, while the height of the bar denotes the unadjusted, two-sided *P* value for the tissue, given on a $-\log_{10}$ scale. *P* values were calculated using a normal null distribution (*z* test) with the mean and variance estimated from 1,000 simulated null *z* scores. Red bars indicate tissues for which enrichment was statistically significant after adjusting for multiple testing (false discovery rate < 0.05). CNS, central nervous system. **b**,**c**, Results from the luciferase assay in HepG2 cells for the *HMBS* promoter fragments HMBS_P2 (**b**) and HMBS_P1 (**c**). For each set of alleles, the box plots represent the median, interquartile range, and minimum and maximum values of all replicates, where *n* is the number of independent plasmid extractions multiplied by the number of independent transfections. The *P* values (two-sided *t*-test) represent pairwise differences in means, either between the control plasmid pGL4.10 without any insert and the plasmid with one of the fragments inserted, or between the two plasmids with fragments inserted. In **b**, AT denotes the fragment that contains the rs1799993-A and rs1006195-T alleles, while CG denotes the fragment with the rs1799993-C and rs1006195-G alleles. **c** shows the results for the smaller *HMBS* promoter fragment (HMBS_P1), which only includes rs1006195. This fragment did not show any promoter activity, and no difference between the alleles (G and T) was observed. We therefore conclude that rs1799993 is the most likely functional variant on the HMBS_P2 fragment. **d**, GTEx data of the genotype-dependent gene expression in VAT for the genotypes of rs1799993, where *n* denotes the number of biologically independent samples for each genotype. The violin plots show the median (white line), interquartile range (gray box) and distribution (black area) of the normalized expression levels for the different alleles. The rs1799993-A allele is associated with increased expression levels of *HMBS*, which is consistent with the results from the luciferase assay, where the fragment (AT) that contains rs1799993-A and rs1006195-T has a higher promoter activity.

Table 8). Altogether, common genetic variants explained 37.3% and 38.5% of the variation in VAT^ in females and males, respectively. The high SNP heritability suggests that visceral fat is more heritable than other anthropometric traits, such as waist circumference, which has a reported[14] SNP heritability of merely $h^2 = 15 \pm 5\%$. We note that the genomic inflation was 1.108 in the combined cohort, which appears to be a result of true underlying associations, and not due to population structure (Supplementary Text).

There was an overlap between VAT^-associated loci and loci associated with other adiposity-related phenotypes (Supplementary Table 9). The overlap with BMI and waist circumference was generally more pronounced compared with the overlap with hip circumference and waist-to-hip ratio adjusted for BMI (WHRadjBMI). Also, the genetic correlations (r_g) between VAT^ and other adiposity-related phenotypes were generally high ($r_g \geq 0.84$), with the exception of WHRadjBMI (Supplementary Table 9). This is in line with previous work[15], which found genetic correlations between various adiposity-related traits to lie in the range $r_g = 0.77–0.95$.

GWA signals were enriched for genes expressed in brain tissues and the central nervous system (Fig. 1a and Supplementary Table 10). This implies that VAT is mainly a 'behavioral trait', as was previously proposed for BMI[16]. Among the most significant Reactome pathways (Supplementary Table 11), we found several that relate to the release of well-known neurotransmitters, such as dopamine, serotonin, acetylcholine, norepinephrine and glutamate, as well as pathways for the integration of energy metabolism and inhibition of insulin secretion. One significant Kyoto Encyclopedia of Genes and Genomes pathway was the type 2 diabetes mellitus pathway, which is represented by a subset of the same genes as the Reactome inhibition of insulin secretion pathway.

Among our GWA hits, overlap with an expression quantitative trait locus (eQTL) was identified for 71 of the 209 VAT^-associated lead SNPs (Supplementary Tables 8 and 12). No fewer than 47 SNPs were also in high ($R^2 > 0.8$) linkage disequilibrium with missense variants, of which five are predicted to be deleterious/damaging both by PolyPhen and SIFT (Supplementary Tables 8 and 13).

	Females	Males
Hypertension	**37,287/123,650**	**50,656/113,089**
Unadjusted VAT^	3.13 (3.06–3.19)	1.97 (1.95–2.00)
Adjusted VAT^	2.80 (2.73–2.86)	1.88 (1.86–1.91)
Bias-corrected VAT^	3.41 (3.32–3.50)	2.17 (2.14–2.21)
Measured VAT	2.92 (2.33–3.66)	1.81 (1.61–2.04)
Rank-transformed VAT^	1.89 (1.87–1.92)	1.81 (1.79–1.84)
Heart attack/angina	**3,467/157,470**	**11,383/152,362**
Unadjusted VAT^	2.46 (2.35–2.57)	1.60 (1.57–1.63)
Adjusted VAT^	2.22 (2.10–2.34)	1.49 (1.46–1.53)
Bias-corrected VAT^	2.45 (2.31–2.60)	1.61 (1.57–1.65)
Measured VAT	1.62 (0.72–3.65)	1.34 (1.05–1.71)
Rank-transformed VAT^	1.78 (1.71–1.86)	1.50 (1.47–1.54)
Type 2 diabetes	**4,670/154,511**	**10,002/150,830**
Unadjusted VAT^	5.04 (4.84–5.24)	2.50 (2.45–2.55)
Adjusted VAT^	4.95 (4.74–5.17)	2.43 (2.38–2.49)
Bias-corrected VAT^	5.79 (5.52–6.08)	2.80 (2.73–2.88)
Measured VAT	8.55 (4.48–16.3)	2.01 (1.56–2.58)
Rank-transformed VAT^	3.56 (3.43–3.69)	2.61 (2.54–2.67)
Hyperlipidemia	**15,333/145,835**	**25,681/138,303**
Unadjusted VAT^	2.38 (2.32–2.44)	1.54 (1.52–1.56)
Adjusted VAT^	2.09 (2.03–2.16)	1.45 (1.43–1.48)
Bias-corrected VAT^	2.36 (2.28–2.44)	1.57 (1.54–1.60)
Measured VAT	2.06 (1.53–2.77)	1.42 (1.24–1.62)
Rank-transformed VAT^	1.68 (1.64–1.71)	1.47 (1.44–1.49)

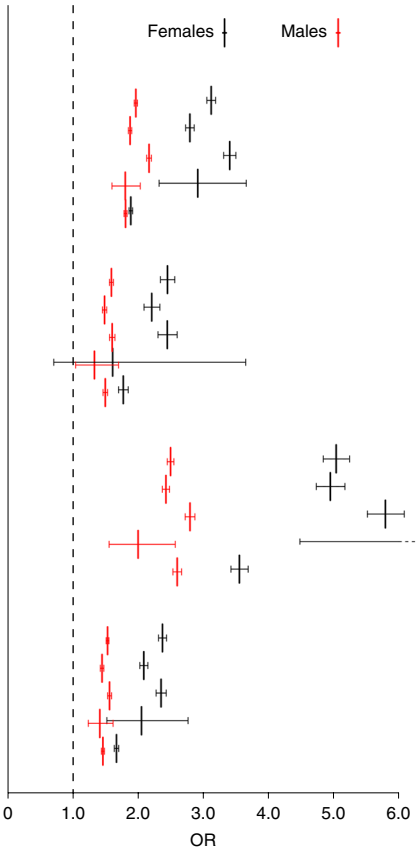

Fig. 2 | VAT^ in relation to cardiovascular and metabolic diseases. ORs and 95% CIs (normal approximation) are shown for females and males separately. The numbers in bold denote the total numbers of cases/controls for each disease and sex. However, for measured VAT, the numbers of cases/controls for females and males, respectively, are: 352/1,337 and 562/1,322 (hypertension); 25/1,664 and 93/1,791 (heart attack/angina); 31/1,636 and 67/1,790 (type 2 diabetes); and 168/1,526 and 338/1,547 (hyperlipidemia). Unadjusted VAT^ denotes the OR per unit increase (1 kg) in VAT^ in relation to disease, not adjusting for any covariates. Adjusted VAT^ denotes the OR when adjusting for covariates. Bias-corrected VAT^ denotes the corresponding OR when correcting VAT^ for measurement errors (covariate-adjusted model). Since the random error in VAT^ was higher in males compared with females (Supplementary Table 4), there was a concern that the observed differences in ORs between sexes were, to a large extent, artifacts caused by differences in measurement error. However, bias-corrected results from SimEx simulations do not support this view, as the differences in ORs between the sexes for the bias-corrected VAT^ tend to be larger, rather than smaller. Measured VAT denotes the OR per unit increase (1 kg) in VAT as measured by DXA in a small subset of the cohort (covariate-adjusted model). The ORs appear not to be strongly affected by any systematic error in VAT^, as the ORs for measured VAT do not differ significantly from those of VAT^. Finally, rank-transformed VAT^ denotes the OR per unit standard deviation in ranks, based on the covariate-adjusted model, with VAT^ being rank-transformed to standard normal distributions for females and males separately. As the significant results remained significant even after VAT^ was rank-transformed, we conclude that the difference in effect between males and females is not only due to the difference in average VAT mass between the sexes.

One of the novel GWA loci was *HMBS*, which is linked to adipogenesis via mitochondrial respiratory activity[17]. The associated SNPs of *HMBS* overlapped with an eQTL for *HMBS* in VAT, which suggests that gene regulation might mediate the association. A subset of novel variants, including the associated *HMBS* SNPs, were therefore selected for functional follow-up (Extended Data Fig. 5) to test for difference in luciferase activity between alleles in HepG2 cells (Supplementary Table 14 and Extended Data Fig. 6). Interestingly, one SNP in the regulatory region of *HMBS* (rs1799993) was associated with a clear difference in activity of the *HMBS* promoter (Fig. 1b,c). The allele (A) that was associated with higher promoter activity was also associated with both increased expression of *HMBS* (Fig. 1d) and increased VAT^ (Supplementary Table 12), which is consistent with the concept that increased expression of *HMBS* may lead to stimulation of adipogenesis[18] and subsequent expansion of adipose tissue, thereby increasing the depot of visceral fat.

VAT^ was strongly associated with increased risk for hypertension, hyperlipidemia, type 2 diabetes and heart attack/angina (Fig. 2). The associations were stronger ($P < 0.0001$) in females compared with males for all four diseases (Supplementary Table 15), which is consistent with previous studies[1], and the largest difference in odds ratio (OR) between the sexes was found for type 2 diabetes (Fig. 2). This difference in effect size is unlikely to be an artifact of any systematic error in VAT^ (Supplementary Text), and it remained after accounting for measurement errors in VAT^ and after adjusting for differences in the VAT^ distribution between sexes (Fig. 2). Apart from being a strong predictor of disease, VAT^ also exhibited an effect independent of BMI (Supplementary Table 16). All BMI-adjusted ORs remained significantly larger than unity. The *P* value for VAT^ was also smaller than the corresponding *P* value for BMI in all cases except for hypertension in males. Furthermore, our results point towards important differences in the effect of VAT^ between type 2 diabetes subgroups with specified medical complications (Extended Data Fig. 7). For example, a significantly higher OR was estimated in type 2 diabetics with renal complications compared with type 2 diabetics diagnosed with ketoacidosis.

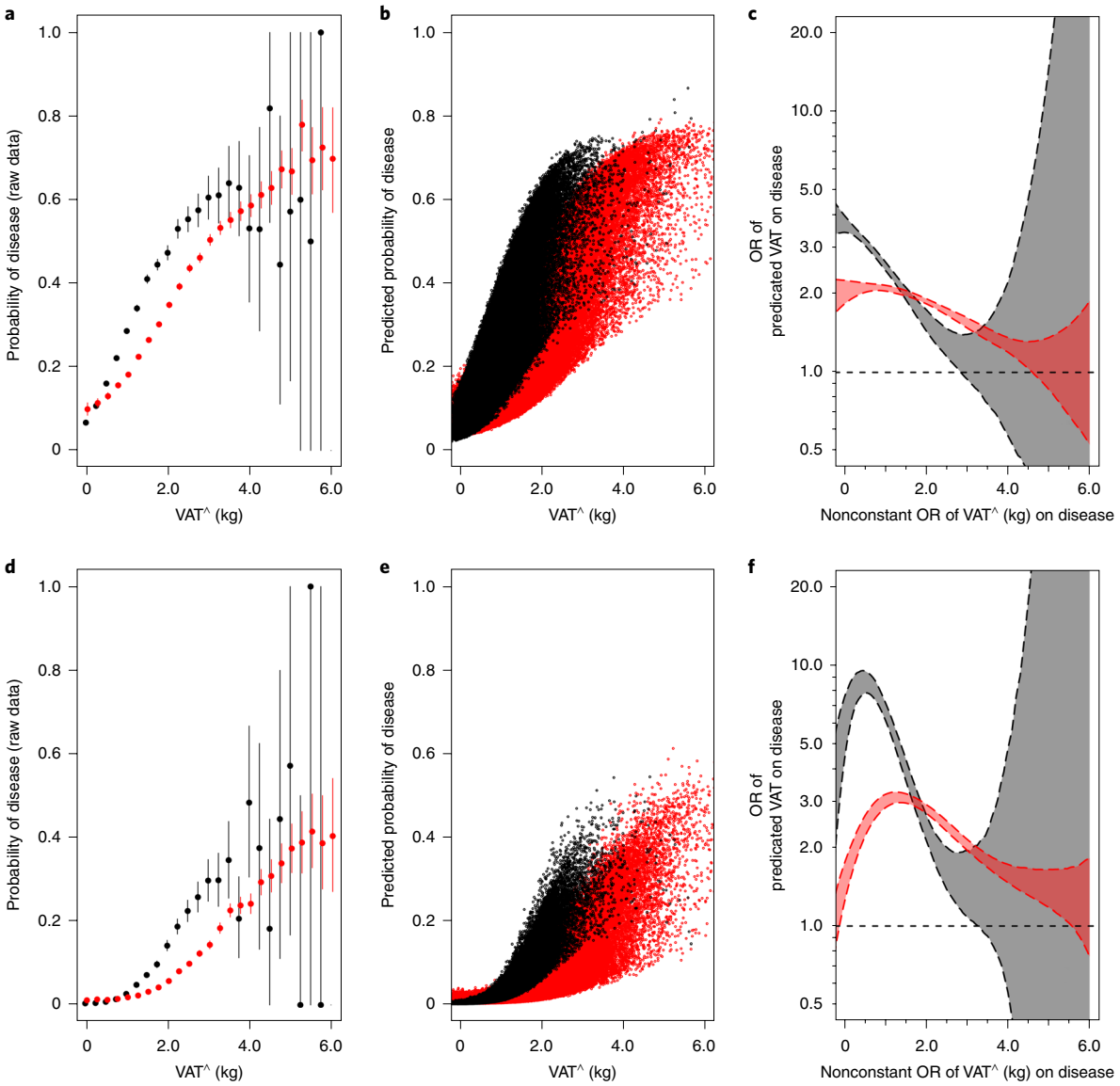

Fig. 3 | Polynomial logistic regression and the change in OR with increasing VAT^. a–f, Models for hypertension (**a**–**c**) and type 2 diabetes (**d**–**f**), showing the observed probability (absolute risk) of having been diagnosed with disease, without adjusting for any covariates (**a** and **d**), the predicted probability (absolute risk) of disease for each individual (**b** and **e**), given the adopted polynomial model with covariates (Supplementary Table 17), and the nonconstant ORs (that is, 95% basic bootstrap CIs) for the adopted polynomial model (**c** and **f**) for a one-unit (1 kg) increase in VAT^, each as a function of VAT^, for females (black and gray) and males (red and pink) separately. Error bars in **a** and **d** indicate 95% CIs, assuming that the numbers of cases and controls in each VAT^ bin are distributed according to two independent Poisson distributions. The total numbers of cases and controls for hypertension and type 2 diabetes are given in Fig. 2 for females and males separately. Note that at high VAT^, the data are too sparse to adequately constrain the OR, which leads to inflated CIs. The nonlinear results presented here were not sensitive to the adopted polynomial in VAT^ (Extended Data Fig. 9).

Such differences can affect risk assessment, and are consistent with the concept of type 2 diabetes being a heterogeneous disease that can be divided into several distinct subclasses[19].

By relaxing the assumption of linearity, a significant nonlinear effect ($P < 0.0001$) of VAT^ on disease was uncovered for all four cardiometabolic diseases (Fig. 3, Extended Data Fig. 8 and Supplementary Table 17). This finding was also supported by the data for VAT mass, as measured by DXA (Supplementary Table 18 and Supplementary Text). A nonconstant OR (Supplementary Text) was observed in the sense that a one-unit (1 kg) increase of VAT^ was generally associated with a more pronounced increase in disease risk, as reflected by a higher OR, in individuals with small or moderate depots of VAT compared with individuals with large depots of VAT. Ultimately, a saturation of the disease risk appears to occur at high VAT^ for all four diseases, at which the OR approaches unity (Fig. 3 and Extended Data Figs. 8 and 9). However, in contrast with the other diseases that chiefly exhibited monotonically decreasing ORs, type 2 diabetes was found to exhibit a pronounced peak in the nonconstant OR, with the risk of disease remaining low at low VAT^ (Fig. 3f). This allowed us to define a sex-specific 'VAT transition point', VAT_{tr} (Supplementary Text), above which the risk for type 2 diabetes rapidly increased, before saturation. We estimated VAT_{tr} to be 1.31 kg (95% CI = 1.23–1.41 kg) for females and 2.06 kg (95% CI = 1.93–2.19 kg) for males. As many as 33% of the white British males and 16% of the females had a VAT^ above VAT_{tr} in the UKBB. This transition point is aimed for use in the clinic to identify individuals at risk of developing type 2 diabetes. Moreover, the absolute risk of type 2

Table 1 | MR estimates of the causal effects of VAT^ on cardiometabolic diseases

Disease	Design	Females				Males			
		Cases	Controls	OR/intercept (95% CI)	*P* value[c]	Cases	Controls	OR/intercept (95% CI)	*P* value[c]
Hypertension	Two sample[a]	25,414	85,171	2.61 (2.14–3.19)	3.1×10^{-21}	33,744	76,216	1.86 (1.65–2.10)	1.4×10^{-24}
	One sample[a]			3.51 (2.71–4.54)	2.5×10^{-21}			2.00 (1.75–2.28)	4.5×10^{-24}
	MR-Egger intercept[b]			−0.002 (−0.016–0.011)	0.75			−0.009 (−0.026–0.008)	0.31
Heart attack/angina	Two sample[a]	2,259	108,326	1.38 (0.79–2.42)	0.25	7,484	102,477	1.73 (1.42–2.11)	3.8×10^{-8}
	One sample[a]			1.58 (0.76–3.27)	0.22			2.00 (1.58–2.54)	6.9×10^{-9}
	MR-Egger intercept[b]			0.027 (−0.002–0.056)	0.072			−0.002 (−0.026–0.023)	0.89
Type 2 diabetes	Two sample[a]	3,044	106,371	7.34 (4.48–12.0)	2.7×10^{-15}	6,473	101,623	2.50 (1.98–3.14)	6.4×10^{-15}
	One sample[a]			13.5 (7.08–25.6)	2.4×10^{-15}			4.05 (3.14–5.23)	9.1×10^{-27}
	MR-Egger intercept[b]			−0.015 (−0.039–0.010)	0.24			−0.015 (−0.042–0.012)	0.27
Hyperlipidemia	Two sample[a]	10,317	100,432	1.69 (1.27–2.24)	2.9×10^{-4}	17,029	93,101	1.35 (1.18–1.55)	1.7×10^{-5}
	One sample[a]			2.01 (1.39–2.91	2.1×10^{-4}			1.54 (1.31–1.82)	3.1×10^{-7}
	MR-Egger intercept[b]			0.001 (−0.037–0.040)	0.95			−0.017 (−0.046–0.013)	0.27

[a]ORs with corresponding CIs represent generalized least squares estimates from the GSMR analysis[21], based on 44 genome-wide significant ($P<5\times10^{-8}$) lead SNPs identified in a GWAS performed in the interim release of the UKBB genotype dataset (Supplementary Table 21). All ORs are given per 1kg increase in VAT^. Results from the main, two-sample MR design are generally conservative and the effects are probably underestimated, partly due to the fact that any weak-instrument bias is in the direction of the null[22] and partly due to 'winner's curse' bias. Note that any remaining dependence between the two cohorts in the two-sample design is unlikely[23] to introduce weak-instrument bias in the direction of the confounded association. The causal estimate from the one-sample design may be interpreted as an upper limit to this bias. In some cases, a few SNPs have been removed from the analysis, as they were flagged as pleiotropic outliers (Supplementary Table 22). [b]Evidence of directional pleiotropy is present only if the MR–Egger intercept deviates significantly from zero. [c]Unadjusted and two-sided *P* values, estimated from a standard normal null in logit space (marginal *z* test), are reported. Values below $P=3.2\times10^{-3}$ (Šidák correction for 16 tests) are considered statistically significant, assuming independence between sexes, diseases and the effect and intercept estimates.

diabetes and hypertension was on average higher in females compared with males with the same VAT^ (Fig. 3a,d). This excess risk in females was observed for a wide range of VAT^ values, despite the fact that both the average VAT mass (Supplementary Table 2) and the prevalence of disease (Fig. 2) was higher in males. This shows that VAT is a stronger risk factor in females, while the higher overall prevalence of disease in males is probably due to their larger average depot of visceral fat.

The associations between VAT^ and risks for disease were verified in a two-sample Mendelian randomization (MR) analysis (Table 1). With the exception of heart attack/angina in females, all estimated causal ORs were significantly above unity ($P\leq0.0003$), suggesting a causal effect of VAT on disease. The causal ORs were also significantly higher in females compared with males for hypertension ($P=0.002$) and type 2 diabetes ($P<0.0001$)—a result that prevailed for type 2 diabetes after accounting for the difference in average mass of visceral fat between females and males (Supplementary Table 19). The causal OR for type 2 diabetes in females was strikingly high (OR = 7.34; 95% CI = 4.48–12.0), and considerable higher compared with what has recently been shown for waist-to-hip ratio adjusted for BMI[20] (Supplementary Text). A statistically significant difference in effect between the sexes could not be established for the remaining diseases due to larger uncertainties in the estimates and/or smaller effect-size differences. Several sensitivity analyses indicated that our MR results were consistent and not affected by pleiotropy (Table 1, Supplementary Table 20 and Extended Data Fig. 10).

In summary, we performed a large-scale GWAS to identify genetic variants that influence VAT. Furthermore, we showed that VAT^, also adjusted for BMI, is strongly associated with disease risk, which suggests that VAT^ captures additional harmful effects not captured by BMI. It is not completely elucidated why VAT is more harmful compared with other fat depots, such as subcutaneous adipose tissue. Possible hypotheses either identify visceral adiposity as being more lipolytic and resistant to the antilipolytic effects of insulin, leading to higher amounts of circulating free fatty acids, or suggest that VAT has a higher rate of macrophage infiltration, which results in a proinflammatory profile that subsequently promotes insulin resistance[3]. Both scenarios generally agree with the causal effect of VAT^ on type 2 diabetes risk. The nonlinear relationship between VAT^ and disease risk should be studied further to gain a deeper understanding of the biology behind the complex relationship between VAT mass and disease.

Online content

Any methods, additional references, Nature Research reporting summaries, source data, statements of code and data availability and associated accession codes are available at https://doi.org/10.1038/s41591-019-0563-7.

Received: 24 April 2018; Accepted: 29 July 2019;
Published online: 9 September 2019

References

1. Fox, C. S. et al. Abdominal visceral and subcutaneous adipose tissue compartments: association with metabolic risk factors in the Framingham Heart Study. *Circulation* **116**, 39–48 (2007).
2. Vega, G. L. et al. Influence of body fat content and distribution on variation in metabolic risk. *J. Clin. Endocrinol. Metab.* **91**, 4459–4466 (2006).
3. Tchernof, A. & Despres, J.-P. Pathophysiology of human visceral obesity: an update. *Physiol. Rev.* **93**, 359–404 (2013).
4. Brown, J. C., Harhay, M. O. & Harhay, M. N. Anthropometrically-predicted visceral adipose tissue and mortality among men and women in the third National Health and Nutrition Examination Survey (NHANES III). *Am. J. Hum. Biol.* **29**, 444–454 (2017).
5. Katzmarzyk, P. T., Mire, E. & Bouchard, C. Abdominal obesity and mortality: the Pennington Center longitudinal study. *Nutr. Diabetes* **2**, e42–e43 (2012).
6. Bentham, J. et al. Worldwide trends in body-mass index, underweight, overweight, and obesity from 1975 to 2016: a pooled analysis of 2416 population-based measurement studies in 128·9 million children, adolescents, and adults. *Lancet* **390**, 2627–2642 (2017).
7. Samouda, H. et al. VAT = TAAT − SAAT: innovative anthropometric model to predict visceral adipose tissue without resort to CT-scan or DXA. *Obesity* **21**, 41–50 (2013).
8. Eastwood, S. V. et al. Estimation of CT-derived abdominal visceral and subcutaneous adipose tissue depots from anthropometry in Europeans, South Asians and African Caribbeans. *PLoS One* **8**, e75085 (2013).
9. Neamat-Allah, J. et al. Validation of anthropometric indices of adiposity against whole-body magnetic resonance imaging—a study within the German European Prospective Investigation into Cancer and Nutrition (EPIC) cohorts. *PLoS One* **9**, e91586 (2014).
10. Neamat-Allah, J. et al. Can the use of blood-based biomarkers in addition to anthropometric indices substantially improve the prediction of visceral fat volume as measured by magnetic resonance imaging? *Eur. J. Nutr.* **54**, 701–708 (2015).
11. Fox, C. S. et al. Genome-wide association for abdominal subcutaneous and visceral adipose reveals a novel locus for visceral fat in women. *PLoS Genet.* **8**, e1002695 (2012).
12. Sung, Y. J. et al. Genome-wide association studies suggest sex-specific loci associated with abdominal and visceral fat. *Int. J. Obes.* **40**, 662–674 (2016).
13. Chu, A. Y. et al. Multiethnic genome-wide meta-analysis of ectopic fat depots identifies loci associated with adipocyte development and differentiation. *Nat. Genet.* **49**, 125–130 (2017).
14. Speed, D. et al. Reevaluation of SNP heritability in complex human traits. *Nat. Genet.* **49**, 986–992 (2017).
15. Sodini, S. M., Kemper, K. E., Wray, N. R. & Trzaskowski, M. Comparison of genotypic and phenotypic correlations: Cheverud's conjecture in humans. *Genetics* **209**, 941–948 (2018).
16. Locke, A. E. A. E. et al. Genetic studies of body mass index yield new insights for obesity biology. *Nature* **518**, 197–206 (2015).
17. Moreno-Navarrete, J. M. et al. Heme biosynthetic pathway is functionally linked to adipogenesis via mitochondrial respiratory activity. *Obesity* **25**, 1723–1733 (2017).
18. Gómez-Hernández, A., Beneit, N., Díaz-Castroverde, S. & Escribano, O. Differential role of adipose tissues in obesity and related metabolic and vascular complications. *Int. J. Endocrinol.* **2016**, 1216783 (2016).
19. Ahlqvist, E. et al. Novel subgroups of adult-onset diabetes and their association with outcomes: a data-driven cluster analysis of six variables. *Lancet Diabetes Endocrinol.* **6**, 361–369 (2018).
20. Emdin, C. A. et al. Genetic association of waist-to-hip ratio with cardiometabolic traits, type 2 diabetes, and coronary heart disease. *J. Am. Med. Assoc.* **317**, 626–634 (2017).
21. Zhu, Z. et al. Causal associations between risk factors and common diseases inferred from GWAS summary data.*Nat. Commun.* **9**, 224 (2018).
22. Haycock, P. C. et al. Best (but oft-forgotten) practices: the design, analysis, and interpretation of Mendelian randomization studies. *Am. J. Clin. Nutr.* **103**, 965–978 (2016).
23. Burgess, S., Davies, N. M. & Thompson, S. G. Bias due to participant overlap in two-sample Mendelian randomization. *Genet. Epidemiol.* **40**, 597–608 (2016).

Acknowledgements

We acknowledge all of the participants and staff involved in UKBB for their valuable contribution. This research was conducted using the UKBB Resource under application number 15152, following the restrictions on data availability set up by the UKBB. The computations were performed on resources provided by SNIC through the Uppsala Multidisciplinary Center for Advanced Computational Science under projects b2016021 and sens2017538. The research was funded by the Swedish Society for Medical Research (M.R.-A. and Å.J.), Swedish Research Council (Å.J., 2015-03327), Kjell and Märta Beijers Foundation (Å.J.), Göran Gustafssons Foundation (Å.J.), Marcus Borgström Foundation (Å.J.), Åke Wiberg Foundation (Å.J., M16-0210), Swedish Heart and Lung Foundation (Å.J., 20170484), Swedish Diabetes Foundation (C.W.) and Science for Life Laboratory (Å.J.).

Author contributions

T.K., M.R.-A. and Å.J. designed the study and performed the data analysis. T.K. developed all of the models, performed the statistical analysis and generated the figures. G.P. and C.W. performed the functional study. T.K., M.R.-A., G.P., J.H., C.W., W.E.E. and Å.J. interpreted the data and wrote the manuscript.

Competing interests

The authors declare no competing interests.

Additional information

Extended data is available for this paper at https://doi.org/10.1038/s41591-019-0563-7.

Supplementary information is available for this paper at https://doi.org/10.1038/s41591-019-0563-7.

Reprints and permissions information is available at www.nature.com/reprints.

Correspondence and requests for materials should be addressed to T.K. or Å.J.

Peer review information: Kate Gao and Brett Benedetti were the primary editors on this article and managed its editorial process and peer review in collaboration with the rest of the editorial team.

Methods

Study cohort. UKBB recruited 502,682 individuals, originally aged 40–69 years, from across the UK during 2006–2010. Most participants were invited once (instance 0), whereas a subset of participants were invited to revisit the assessment center on one or two additional occasions (instances 1 and 2, respectively). Participants were interviewed about lifestyle and disease history via touchscreen questionnaires and verbal interviews. Participants underwent a physical examination that included measurements of weight, height and waist and hip circumference, and females were asked about their menopausal status. Bioelectrical impedance measurements were performed on the Tanita BC418MA body composition analyzer, which uses an eight-electrode setup that estimates body composition in the whole body as well as in the limbs. VAT mass was measured by DXA in a subset of 5,109 individuals at instance 2 using the GE Healthcare Lunar iDXA scanner. This subset of participants was selected independently but was biased towards participants living within a reasonable traveling distance from one of the imaging assessment centers.

Prediction models for VAT mass. Initially, two UKBB subcohorts were constructed: one training dataset with VAT mass measured by DXA (instance 2; $n = 5{,}109$), to which the prediction models were calibrated; and one application dataset (instances 0 and 1; $n = 502{,}638$), in which VAT mass was predicted using the calibrated prediction models. To avoid potential bias due to population structure, only white British participants (data field: 21000; code: 1001) were included in the analysis, and all entries of "do not know", "prefer not to answer" or "NA" for any of the explored predictor variables or in the response were set to missing. After removal, $n = 4{,}212$ participants remained in the training dataset and $n = 397{,}170$ participants remained in the application dataset (Extended Data Fig. 1). The quality control performed on the training dataset included the removal of a number of outliers in the bioelectrical impedance variables. Unfortunately, bioelectrical impedance measurements were only performed at instances 0 and/or 1, in contrast with the other predictors, which were also measured at instance 2. Therefore, all individuals whose BMI had changed by more than eight units between instance 0 or 1 and the instance at which VAT was measured (that is, instance 2) were removed. In total, 14 participants were removed and $n = 4{,}198$ remained after quality control in the training dataset. The same criteria for removal that applied to the training dataset were also applied to the application dataset. Two individuals with inadequate menopausal status were removed, as were two individuals with extremely low waist circumference (≤26 cm) but otherwise average body size measures. Furthermore, a number of individuals with extreme hip circumference in relation to their BMI were removed ($\text{hip} > 2 \times \text{BMI} + 80$ cm), including one male with a hip circumference of 39 cm and a BMI of 23.4 kg m^{-2}. Also, all individuals with a difference in impedance between the left and right arm or the left and right leg of >120 ohm were removed, as were extreme impedance measures in relation to the individual's BMI. As a result of this quality control of the predictors, only 11 individuals with extreme VAT^ had to be removed before the epidemiological studies and GWASs were performed. In total, 950 individuals were removed from the application dataset, whereas $n = 396{,}220$ individuals passed quality control.

We note that individuals in the training dataset were, on average, 4–5 years older than the individuals in the application dataset, in agreement with VAT being measured at a second revisit to the assessment center (instance 2). This difference is reflected in the fraction of females that underwent menopause, as well as in most other variables to different degrees (0.4–4.0% difference in median), and led to a median difference of 6–10% between measured VAT and VAT^ (Supplementary Table 2).

VAT mass was predicted using multiple regression modeling, with a number of predictor interactions, in males and females separately. As discussed in the Supplementary Text, the inclusion of nonlinear terms can be motivated on theoretical and physical grounds. In total, 11 predictor variables distributed on 20 different linear and interaction terms were included in the models (Supplementary Tables 1–3 and Extended Data Fig. 2). The predictors (including the interaction terms) that were incorporated in the prediction models correlated to various degrees with the dependent variable VAT mass. Waist and waist × weight showed the highest correlations with VAT mass for females and males, respectively (Extended Data Fig. 2). For females, the lowest correlation with VAT was height, while for males the lowest correlation was age. The bioelectrical impedance predictors showed significant negative correlations with VAT mass, with whole-body impedance being the most negative, both for females and males (Extended Data Fig. 2).

We created two sets of prediction models in males and females separately: reduced and full models (Supplementary Tables 3 and 4). The full models were based on the entire set of regression terms, with the exception of menopausal status in males. In the two reduced models, only nominally significant terms were selected, while the redundant terms were eliminated by backward elimination. In-sample validation of the models was performed by calculating the predicted R^2 (see Supplementary Text) using two different techniques: leave-one-out cross-validation[24] and bootstrapping. The function validate, in the R package rms, was used to estimate the predicted R^2 by the bootstrap method. The models were further validated (out-of-sample validation) by an independent sample of Irish and other white, non-British individuals from the UKBB. The leave-one-out cross-validation was also used to estimate random and systematic errors of the prediction models (Supplementary Table 4, Extended Data Figs. 3 and 4 and Supplementary Text), while relative goodness-of-fit and model selection were assessed by Akaike's information criterion (AIC). All analyses were done in R version 3.4.2 (ref. [25]) using lm and glm, which are included in the statistics library.

GWAS, enrichment analyses and functional annotation. Genotyping in UKBB was performed using two custom-designed microarrays (UK BiLEVE and Axiom Genotyping), which contain probes for 807,411 and 820,967 SNPs, respectively. Imputation was performed using UK10K and 1000 Genomes phase 3 as reference panels[26,27]. The genetic dataset included 93,093,070 SNPs with imputations from the third release of imputed data from UKBB (version 3; accessed March 2018). As in the filtering of the application dataset for the VAT prediction modeling, only participants of British descent (data field: 21000) were included in the GWA analyses. To minimize the effects of population stratification, an additional filtering included only participants classified as Caucasian by principal component analysis (data field: 22006). Genetic relatedness pairing was provided by the UKBB (data field: 22011). Individuals were excluded due to relatedness based on kinship data (estimated genetic relationship > 0.044), and individuals with a poor call rate (<95%), high heterozygosity (data field: 22010) or sex errors (data field: 22001) were also removed. After filtering, 325,153 participants with VAT^ remained for the GWAS. Of these, 104,271 were part of the interim genotype data release cohort, while 220,882 were part of the second genotype data release of unrelated individuals (Extended Data Fig. 1).

GWA analyses were performed using linear regression models implemented in PLINK version 1.90b3n[28], in females and males separately, while the sex-combined associations were subsequently computed using a fixed-effect meta-analysis. For the main GWAS, SNPs were filtered based on call rate (all SNPs with a call rate > 99% were kept), deviance from Hardy–Weinberg equilibrium accepting SNPs with $P > 10^{-20}$, minor allele frequency (MAF), assuming that MAF > 0.001, and imputation quality (>0.3). After filtering, 10,549,349 SNPs remained. Before the analysis, VAT^ was adjusted for age by the residual method, and rank-transformed using rntransform in the R package GenABEL[29]. The first 15 genetic principal components were included as covariates, together with a batch-effect variable to adjust for genotyping array (Axiom or BiLEVE), as both were used in the first genotype data release (interim release). A family-wise error rate of $\alpha < 0.05$ of the GWAS was ensured by adopting a P value threshold of $P = 3.33 \times 10^{-9}$, accounting for the female, male and sex-combined subgroups, for a MAF threshold of 0.1%, and assuming that genomic inflation due to population structure was absent (see Supplementary Text).

After the GWA analyses, we used the PLINK clump function with thresholds $R^2 = 0.05$, $p_1 = 3.33 \times 10^{-9}$ and $p_2 = 0.0001$, and a window of 2,000 kilobases, to find the lead SNP and define start and end positions for each locus, and to identify multiple uncorrelated SNPs within the locus, if any. If more than one signal was identified within a locus, independence was confirmed for all SNPs by recalculating the conditional P value, adjusting for the most significant SNP(s). The same P value cut-off ($P = 3.33 \times 10^{-9}$) adopted in the GWA analyses, was used in the conditional analyses. A locus was considered as novel for VAT^ if the lead SNP was not in linkage disequilibrium ($R^2 < 0.05$) with any SNP reported in the GWAS Catalog[30] (accessed 1 December 2018) for any of the following adiposity-related phenotypes: VAT, subcutaneous adipose tissue, body fat percentage, BMI, obesity, weight, waist circumference, hip circumference or waist-to-hip ratio. This also included adiposity-related phenotypes adjusted for, for example, BMI, smoking, physical activity and so on, and phenotypes with gene × environment or gene × gene interactions. The variance explained by genetic variants (SNP heritability) was assessed using GCTA version 1.26.0 (ref. [31]). Participants with an estimated genetic relationship > 0.025 were removed from the analysis to evade phenotypic resemblance due to nongenetic effects (for example, shared environment between relatives). Only genotyped SNPs with MAF > 1% and a call rate > 95% ($n = 730{,}616$ SNPs), from the interim release of the UKBB genotype dataset ($n = 104{,}271$ participants in total), were used to estimate the SNP heritability, to avoid confounding effects of uncertainties in the imputed data. Age, a batch indicator variable for the two genotyping arrays and the first ten principal components were included as covariates.

To facilitate the identification of the functional role or tissue specificity for the associated variants, tissue and geneset enrichment analyses were performed using DEPICT version 1.1 (ref. [32]). Geneset enrichment in DEPICT is based on similarities in gene expression. A total of 14,461 so-called reconstituted genesets were pregenerated: genesets that represent a wide set of biological annotations (Gene Ontology (GO), Kyoto Encyclopedia of Genes and Genomes (KEG), Reactome (REA), Mammalian Phenotype (MP), and protein–protein Interaction networks by Ensembl (ENS)). For tissue enrichment in DEPICT, microarray data from 37,427 human tissues were used to group genes with similar expression patterns with regard to different cells and tissues. For the enrichment analyses, we used the data from the sex-combined GWAS in the entire cohort ($n = 325{,}153$). The geneset enrichment analyses identified whether genes related to the most significant ($P < 1 \times 10^{-7}$) GWA hits were over-represented among the reconstituted DEPICT genesets. A false discovery rate below 0.05 was considered significant in the enrichment analyses.

All independent lead SNPs were also functionally annotated with regard to being in linkage disequilibrium with an eQTL or with a missense, splice site, nonsense or frameshift variant. Significant eQTLs were downloaded from the Genotype-Tissue Expression (GTEx) project[33]. First, we selected the subset (80%) of GTEx SNPs that overlapped with the UKBB SNPs. Second, we identified the most significant SNP for each tissue and gene in the GTEx dataset. Third, we estimated the linkage disequilibrium between the lead eQTL SNPs and the independent UKBB lead GWA SNPs. A lead GWA SNP that was in linkage disequilibrium ($R^2 > 0.8$) with a lead GTEx eQTL SNP was considered to be an eQTL for the same gene in the same tissue (Supplementary Table 12). The threshold of significance for the eQTLs was set to 2.3×10^{-9}, in agreement with previous studies[34]. We also used the Bioconductor biomaRt[35] package in R for functional annotation of the lead GWA SNPs. In biomaRt, lead GWA SNPs, and all SNPs in linkage disequilibrium ($R^2 > 0.8$) with the lead SNPs, were cross-referenced against Ensembl Genes and Ensembl Variation version 94 (accessed 29 November 2018, using the human assembly GRCh38), to identify possibly damaging variants such as missense variants, classified as damaging/deleterious with regard to the SIFT and PolyPhen scores, or variants identified as frameshift, stop gained, stop lost or splice acceptor/donor variants (Supplementary Table 13). Before cross-referencing, the GRCh37 coordinates of the SNPs were converted into GRCh38 coordinates using the liftOver tool.

To determine the SNP overlap between our VAT^ GWAS and previous GWASs on other adiposity-related traits, we first searched the GWAS Catalog[30] for known genome-wide significant ($P < 5.0 \times 10^{-8}$) SNPs associated with BMI, waist circumference, hip circumference and WHRadjBMI. We then estimated to what fraction these SNPs were also associated with VAT^ ($P < 5.0 \times 10^{-8}$) in our study. Furthermore, to test whether our novel lead VAT^ SNPs were also associated ($P < 5.0 \times 10^{-8}$) with the above-mentioned traits, we carried out additional GWA analyses for these traits in UKBB, using the same methodology and covariates as for the VAT^ GWAS, except for WHRadjBMI, which was also adjusted for BMI. Genetic correlations (r_g) between VAT^ and BMI, waist, hip and WHRadjBMI were estimated using linkage disequilibrium score regression (LDSC) software[36,37] (version 1.0.0). As for the SNP heritability calculations, only genotyped SNPs from the interim release cohort were used, to avoid introducing bias as a result of imputation errors. Variant filtering and participant quality control were the same as for the main GWA analysis (after filtering, $n = 508{,}171$ SNPs remained for analysis), and sex-stratified SNP associations were calculated from age-adjusted, rank-transformed traits, using a batch indicator variable and 15 principal as covariates, except for the waist-to-hip ratio, which was also adjusted for BMI. As for VAT^, sex-combined associations were estimated using fixed-effect meta-analysis.

Functional analysis. For a subset of the novel VAT^ loci, potentially regulatory SNPs were selected (Extended Data Fig. 5) for functional validation using a luciferase assay in HepG2 cells. The basic criterion for functional follow-up was that the lead SNP overlapped with a GTEx eQTL in adipose tissue. Among these loci, we selected the lead SNP and/or SNPs in linkage disequilibrium ($R^2 > 0.8$), with the lead SNP that was located in regulatory elements identified by histone marks, DNase I hypersensitive sites, or in transcription factor binding sites according to ENCODE or Roadmap epigenomics data. Among the 102 novel adiposity SNPs identified in this study, 20 overlapped with eQTLs in GTEx (Supplementary Table 8). Of these, we selected three loci that overlapped with eQTLs in adipose tissue for genes that have previously been studied specifically in adipocytes: *DPYSL4*, *PKD1* and *VPS11/HMBS*. *DPYSL4* has been shown to regulate energy metabolism in adipocytes and cancer cells through interaction with the mitochondrial supercomplex (a large aggregate of proteins that contains the enzymes of the mitochondrial respiratory chain[38]). *PKD1* encodes polycystin-1, which has been extensively studied due to its association with polycystic kidney disease. *PKD1* encodes a membrane protein that has been proposed to act as a G protein-coupled receptor and mediate mechanosensation in the primary cilium of kidney cells[39]. Polycystin-1 has been studied in adipocyte-derived stem cells, where polycystin-1 has been suggested to influence both adipocyte-derived stem cell proliferation and differentiation activity[40]. *HMBS* is involved in the heme biosynthetic pathway, and expression of this gene is increased during differentiation of adipocytes. *HMBS* has recently been shown to be linked to adipogenesis via mitochondrial respiratory activity[17]. *VPS11* is involved in vesicle-mediated protein trafficking to lysosomal compartments in the cell. *VPS11* has not been linked specifically to adipocyte function; however, the same variants that are associated with *HMBS* expression in adipose tissue are also associated with *VPS11* expression in other tissues.

The *DPYSL4* locus contains 53 SNPs in linkage disequilibrium with the lead GWA SNP, of which three SNPs (rs881347, rs61865793 and rs11146233) overlap with regulatory elements close to the transcription start site of *DPYSL4* (Extended Data Fig. 5c). These SNPs were amplified together in one PCR fragment (Supplementary Table 14). The *PKD1* locus contained 33 SNPs, of which one SNP (rs13337177) is located in a regulatory region in the first intron of *PKD1*, and another SNP (rs36232) is located in a regulatory element upstream of *PKD1*, close to the transcription start site of *RAB26* (Extended Data Fig. 5b). These SNPs were amplified as two nonoverlapping PCR fragments (Supplementary Table 14).

At the *HMBS/VPS11* locus, there were 55 SNPs in the region. Of these, five variants (rs1784461, rs1786141, rs1784460, rs1784459 and rs1786684) overlap with regulatory elements in the *VPS11* promoter, two SNPs (rs1799993 and rs1006195) overlap with regulatory elements in the first intron of *HMBS*, and two SNPs (rs2509121 and rs11217133) overlap with regulatory elements in the promoter of the upstream gene *HYOU1* (Extended Data Fig. 5a). For the *HYOU1* promoter, one PCR fragment amplified both SNPs. For the *HMBS* and *VPS11* promoters, two PCR fragments each were designed (one that included all of the targeted SNPs, and a shorter fragment that included a subset of the SNPs (Supplementary Table 14)).

HepG2 cells were purchased from the American Type Culture Collection and maintained in RPMI-1640 basal medium supplemented with 10% fetal bovine serum and 2 mM L-glutamine, together with 100 units of penicillin and 100 µg streptomycin per 1 ml culture medium. Cells were plated 1 d before transfection in 96-well plates. The confluency was around 70% on transfection. Each well was transfected with 0.3 µl X-tremeGENE HP DNA transfection reagent (Roche) and 100 ng experimental firefly luciferase reporter plasmid, and 1 ng of pGL4.74 *Renilla* luciferase reporter plasmid was used as an internal control for monitoring transfection and lysis efficiency. Cells were harvested 24 h after transfection and assayed with the Dual-Luciferase Reporter Assay System (Promega) on an Infinite M200 PRO reader (Tecan).

For each SNP that was selected for functional analyses, DNA samples from two individuals who were homozygous for different alleles were selected from a cross-sectional cohort from Sweden[41]. PCR primers were designed to amplify the regions of interest, and the products were cloned into plasmids employing the In-Fusion cloning system (Takara). To test for enhancer activity, the putative enhancer element with variations was inserted upstream of the minimal promoter sequence of pGL4.23. To test for promoter activity, fragments with sequence variants were inserted into pGL4.10 directly upstream of the luciferase gene. All inserts were verified by Sanger sequencing. Two to three independent plasmid extractions and transfections were performed, and the data are presented as ratios of the firefly luciferase activity from the experimental plasmids to *Renilla* luciferase activity from pGL4.74.

Six out of eight plasmids were successfully constructed and verified by Sanger sequencing (Supplementary Table 14). Generically, three independent plasmid extractions were performed from each fragment, and for each extraction three independent transfections were carried out. Only one fragment (HMBS_P1) failed to show any promoter or enhancer activity (Extended Data Fig. 6). One of the fragments (HMBS/VPS11_HMBS_P2), which harbored rs1799993 and rs1006195, showed a significant difference ($P < 0.05$) in promoter activity between alleles (Extended Data Fig. 6b), which was verified by six additional independent transfection experiments (Fig. 1b).

Epidemiological study. We analyzed four different disease phenotypes: type 2 diabetes, heart attack/angina, hypertension and hyperlipidemia. Disease cases and controls were selected based on the touchscreen questionnaire data and verbal interviews. Participants who reported that they did not know or preferred not to answer the questions in the respective data field were set as missing. Type 2 diabetes cases were extracted from the main and secondary International Classification of Diseases 10 (ICD-10) summary information on diagnoses (data fields: 41202 and 41204). Cases were selected as participants with non-insulin-dependent diabetes mellitus. In addition, participants reporting that they had type 2 diabetes in the verbal interview (data field: 20002; code: 1223) were also selected as cases. Participants reporting that a doctor had told them that they had diabetes of any other type in the verbal interview (data field: 20002; code: 1220, 1221 or 1222) and participants reporting that a doctor had told them that they had (unspecified) diabetes (data field: 2443) were set as missing, as long as they had not been selected as cases from the ICD-10 summary information. The rest were set as controls. Hypertension cases were selected as participants reporting that a doctor had told them that they had high blood pressure (data field: 6150). Participants who responded "no" were used as controls. Heart attack or angina cases were selected as participants reporting that a doctor had told them that they had had a heart attack or angina (data field: 6150). Participants who responded "no" were used as controls. Finally, hyperlipidemia cases were selected as participants who indicated that they had high cholesterol levels during the verbal interview (data field: 20002). Participants who responded that they did not have high cholesterol were used as controls.

In this study, we primarily focused on the biology of visceral fat and its implications for disease development, with special attention to sex differences. We therefore chose to express VAT^ in physical units (kg), to allow for straightforward interpretation of the results. A direct comparison between the sexes is not possible if VAT^ is standardized for females and males separately. Direct comparisons with other adiposity-related traits were of lesser concern. Besides, measurements in physical units can instantly be used in a clinical setting. Nonetheless, we also estimated 're-scaled' ORs, which were conditional on the respective distribution in VAT^. This was done before the analysis by rank-transforming VAT^ for females and males separately to standard normal distributions, using rntransform within the R package GenABEL[29]. This particular transformation was chosen to account for the general difference in distribution between sexes, and not only for the difference in mean (shift) and variance (scale), as in the case of the

z transformation (see Supplementary Text). Unless otherwise stated, all ORs refer to an increase of 1 kg in VAT^. Note that P values for ORs, given the null hypothesis of no association, are invariant under the z transformation.

To test whether VAT mass was associated with cardiovascular and metabolic disease, we performed logistic regression using VAT^ as the predictor variable and disease status as the response. Males and females were analyzed separately, and age, smoking behavior (never, former, and heavy or occasional present smokers), as well as the first 15 genetic principal components, were included as covariates. The linear logistic modeling was done in R version 3.4.2 (ref. [25]) using glm, included in the stats library. A potential difference in OR between females and males was assessed by modeling the effect on disease of a sex × VAT^-interaction term in a sex-combined analysis. The null hypothesis of no difference in the effect of VAT^ on disease between females and males is equivalent to the hypothesis that the coefficient of the interaction term is equal to zero, which was tested by a marginal t-test. The dichotomous sex variable was coded as ("female", "male") = (0, 1), and the usual covariates of the adjusted models were included.

To assess whether VAT^ could explain the risk of disease independent of BMI, we performed a logistic regression including BMI as a covariate, in addition to age, smoking history and the first 15 principal components. Note that adjusting for BMI in the logistic regression models could possibly introduce collider bias. However, in its simplest form, collider bias generally induces a negative correlation or reduces a positive effect, which is referred to as Berkson's paradox[42]. The remaining observed positive effect of VAT^ on disease after adjusting for BMI should therefore, in the presence of such a particular bias, constitute a lower limit to the true effect.

The effect of VAT^ on the risk of type 2 diabetes, conditional on specified complications, was assessed using the information on medical complications related to type 2 diabetes from the ICD-10 classification of diseases, present in UKBB. Cases were divided into seven different subgroups with specified complications, including type 2 diabetes cases with: (1) coma; (2) ketoacidosis; (3) renal complications; (4) ophthalmic complications; (5) neurological complications; (6) peripheral circulatory complications; and (7) no complications. Females and males were analyzed separately and the same individuals as in the main analyses were used as controls.

We also tested whether a significant nonlinear effect of VAT^ was present in the data. We explored this possibility assuming the log odds to be a polynomial function of VAT^. The logit function was then taken to be of the form:

$$\mathrm{logit}(p(x; z_1, \ldots, z_m)) = f(x; \boldsymbol{z}) = \beta_0 + \beta_1 x + \beta_2 x^2 + \ldots + \beta_q x^q + g(\boldsymbol{z})$$

where x denotes VAT^, q is the degree of the polynomial, and $g(\boldsymbol{z})$ denotes the adopted function of covariates. To test for a nonlinear effect, we compared the AIC of models with ($q > 1$) and without ($q = 1$) higher-order polynomial terms in VAT^. Aside from smoking behavior and the first 15 genetic principal components, we also included polynomial terms for age (that is, in case the AIC decreased by a significant amount when a higher-order polynomial term in age was included in the model). A sensitivity test of the nonlinear effect on the degree of the polynomial in VAT^ was also performed (Extended Data Fig. 9 and Supplementary Text). See Supplementary Text for a definition of the nonconstant OR and a derivation of the VAT transition point. As for the linear modeling, the polynomial logistic modeling was done in R version 3.4.2 using glm.

Causal inference by MR. MR is an instrumental variable approach used in observational epidemiology to obtain consistent estimates of putative causal relationships. The method is applied when unmeasured or unknown confounding and/or reversed causation is suspected to bias the estimated association between exposure and outcome. In reality, it is a daunting task to measure, or even be aware of, all covariates that can affect both exposure and outcome, wherefore MR is an attractive alternative. The MR method gives a consistent estimate of the causal relationship between exposure and outcome if the genetic variants used in the analysis are valid instruments. A genetic variant is a valid instrument if: (1) the variant is associated with the exposure; (2) the variant is not associated with any measured or unmeasured confounder; and (3) the variant is associated with the outcome only via the exposure (that is, the variant is independent of the outcome, given the exposure (and confounders)). The third assumption is referred to as the exclusion restriction. Assumptions (2) and (3) are strong and cannot be directly tested. The violation of these two assumptions introduces pleiotropy and may result in biased causal estimates.

To assess whether any effect of VAT^ on disease was biased by unmeasured confounding, we performed a sex-stratified, two-sample MR analysis. Instrumental variable selection of strong genetic variants was performed by conducting a sex-combined GWAS on VAT^ in the subcohort ($n = 104{,}271$) of the interim release UKBB genotype dataset (Extended Data Fig. 1). As in the main GWAS of the combined cohort, we used the imputed genotype data from the third release (data accessed March 2018). After clumping (using the clump function in PLINK) with a linkage disequilibrium threshold of $R^2 = 0.1$ and a window of 2,000 kilobases, 44 genome-wide significant ($P < 5 \times 10^{-8}$), nearly independent lead SNPs were identified (Supplementary Table 21). These variants were then selected as the genetic instruments of the MR analyses. The same subcohort (interim release) was used to estimate the sex-specific effects of the genetic instruments on VAT^.

A second, nonoverlapping and unrelated dataset ($n = 220{,}882$) of UKBB participants (Extended Data Fig. 1) was used to estimate the effects of the instrumental variables on risk of disease. Since our exposure is a predicted variable, there was a concern that additional pleiotropy could have been introduced by the sheer complexity of the prediction models, defining VAT^. To account for potential pleiotropy in our data, the main MR analysis was performed with the R package gsmr[21] (version 1.0.7), which identifies and removes pleiotropic outliers before causal effect estimation. The generalized summary-data-based MR (GSMR) method[21] utilizes the generalized least squares technique to estimate putative causal effects, which is a regression approach that allows for both heteroskedastic and correlated data via the variance–covariance matrix. The linkage disequilibrium correlations between the nearly independent SNPs were estimated from 5,000 randomly selected white British individuals in the UKBB. The significance threshold for a SNP being identified as a HEIDI-outlier[21] (that is, being invalid) was set to the default value of $\alpha = 0.01$. Any SNP below this threshold was removed before the MR analysis (Extended Data Fig. 10 and Supplementary Table 22). To avoid potential collider bias, we only used age and the first 15 principal components as covariates in all MR models.

Several alternative MR methods that are robust to the presence of invalid instruments, including the weighted median approach[43] and MR Egger[44] were also performed in a sensitivity analysis (Supplementary Table 20), as described in the Supplementary Text. These analyses were performed in the R package MendelianRandomization (version 0.4.1). In addition, a one-sample MR using the second dataset only was performed to assess the effect of weak-instrument and winner's curse bias in the GSMR and weighted median approaches (Supplementary Text).

Statistical analyses. Apart from the prediction modeling and the main GWA, epidemiological and MR analyses, which are described in their respective subsections, we performed a number of additional statistical analyses and tests. CIs of the coefficients, adjusted coefficients and predicted coefficients of determination (Supplementary Text) of the VAT^ prediction models were estimated by basic bootstrapping using a minimum of 50,000 bootstrap samples. Likewise, the 95% confidence bands of the nonconstant ORs (see Fig. 3c,f and Extended Data Fig. 8c,f) were estimated by basic bootstrapping using 1,000 bootstrap samples. We estimated all parameters in the polynomial logistic regression model (Supplementary Table 17) and calculated the nonconstant OR for the original sample and for each bootstrap sample. For any given VAT^, the 95% basic bootstrap CI was then governed by:

$$I = \left(2\widehat{\mathrm{OR}(x)} - q_{0.975}, 2\widehat{\mathrm{OR}(x)} - q_{0.025}\right)$$

where $\widehat{\mathrm{OR}(x)}$ denotes the estimate of the nonconstant OR at $x = \mathrm{VAT}^\wedge$ (that is, from the original sample), while $q_{0.975}$ denotes the 97.5% quantile and $q_{0.025}$ denotes the 2.5% quantile of the sample of bootstrapped, nonconstant ORs. In a similar manner, we also estimated the 95% CIs of the 'VAT transition points' for type 2 diabetes (Supplementary Text), with basic bootstrapping using 1,000 bootstrap samples.

The 95% CIs of the observed probability (absolute risk) of being diagnosed with disease, conditional on VAT^, in the population of white British individuals (for example, Fig. 3a,d) were estimated first by assuming that the numbers of cases and controls in each VAT^ bin were distributed according to two independent Poisson distributions, such that:

$$X_i \sim \mathrm{Pois}\left(\lambda_i = n_{i,\mathrm{cases}}\right)$$

and:

$$Y_i \sim \mathrm{Pois}\left(\mu_i = n_{i,\mathrm{controls}}\right)$$

where $n_{i,\mathrm{cases}}$ and $n_{i,\mathrm{controls}}$ are, respectively, the numbers of cases and controls in VAT^ bin i. The error distribution, Z_i, is then taken to be of the form:

$$Z_i \overset{D}{=} \frac{X_i}{X_i + Y_i}$$

The 95% CI of bin i was finally estimated by computing the 2.5 and 97.5% quantiles of an empirical error distribution function, corresponding to Z_i and generated by 10,000 random variates x_i and y_i, which were drawn from the two Poisson distributions X_i and Y_i, respectively.

The predicted probability of disease, p_j, for each individual, j, given a (nonlinear) logistic regression model with estimated parameters $\hat{\beta}_0, \hat{\beta}_1, \ldots$, is given by the expression:

$$p_j = \frac{1}{1 + e^{-f(x_j; \boldsymbol{z}_j)}}$$

where:

$$f(x_j; \boldsymbol{z}_j) = \hat{\beta}_0 + \hat{\beta}_1 x_j + \ldots + \hat{g}(\boldsymbol{z}_j)$$

and where x_j is the VAT^ of individual j, and z_j is the vector of covariates of individual j. These predictive probabilities were calculated for females and males separately (see, for example, Fig. 3b,e).

To assess the amount of bias introduced by the non-negligible measurement errors in VAT^ (Fig. 2), we performed errors-in-variables modeling using the SimEx algorithm, implemented in the R package simex. As a measure of the error in VAT^, we adopted the estimated maximum standard deviation (see Supplementary Table 4) for each subgroup. The vector of λs for which the simulation step was performed was set to $\lambda = (0.25, 0.5, 0.75, 1.0, 1.25, 1.5, 1.75, 2.0)^{\mathrm{T}}$, while the number of iterations for each λ was set to $B = 400$. In the extrapolation step, a quadratic fitting method was used.

Under $H_0 : \beta_2 = 0$, there is no nonlinear (quadratic) term for measured VAT in the logistic regression. If so, there should be an equal probability to obtain an estimate $\hat{\beta}_2 > 0$ as to obtain an estimate $\hat{\beta}_2 < 0$ (Supplementary Table 18). The null distribution is thus given by the binomial distribution such that $X \sim \mathrm{Bin}(n, p)$, with $p = 0.5$ and where n is the total number of independent tests. Now, assuming that the four diseases are independent in both females and males, we have $n = 8$, and the probability that we should observe at least seven events in which $\hat{\beta}_2 < 0$ simply by chance is given by $\mathbb{P}(X \geq 7) = 0.035$.

When testing for equality of the causal OR between sexes in the MR analysis, we assumed a one-tailed z test for unequal variances (normal approximation), with the alternative hypothesis being:

$$H_1 : \beta_{\mathrm{F}} > \beta_{\mathrm{M}}$$

where β_{F} and β_{M} denote the causal estimates of VAT^ on disease in females and males, respectively. This was done to incorporate previous evidence of the relationship between females and males, as suggested by the results from the epidemiological study (Fig. 2).

Ethics committee approval. Ethical approval was given to the UKBB resource by the North West Multicentre Research Ethics Committee (covering the United Kingdom), National Information Governance Board for Health and Social Care (covering England and Wales) and Community Health Index Advisory Group (covering Scotland). UKBB possesses a generic Research Tissue Bank approval granted by the National Research Ethics Service, which lets applicants conduct research on UKBB data without obtaining separate ethical approvals. Written consent was obtained from all UKBB participants.

Reporting Summary. Further information on research design is available in the Nature Research Reporting Summary linked to this article.

Data availability

The data on which this study is based (application number 15152) are available for bona fide researchers from the UKBB Resource (http://www.ukbiobank.ac.uk/about-biobank-uk/), on filing an application to the UKBB. The data for VAT^ can be accessed via the UKBB Resource, while the summary statistics of the GWAS are available for download from the GWAS Catalog (https://www.ebi.ac.uk/gwas/). Relevant additional data will be available from the authors on request.

References

24. Hastie, T., Tibshirani, R. & Friedman, J. *The Elements of Statistical Learning: Data Mining, Inference, and Prediction* (Springer, 2001).
25. R Core Development Team *R: A Language and Environment for Statistical Computing* (R Foundation for Statistical Computing, 2016).
26. Walter, K. et al. The UK10K project identifies rare variants in health and disease. *Nature* **526**, 82–90 (2015).
27. Auton, A. et al. A global reference for human genetic variation. *Nature* **526**, 68–74 (2015).
28. Weeks, J. P. plink: An R package for linking mixed-format tests using IRT-based methods. *J. Stat. Softw.* **35**, 1–33 (2010).
29. Aulchenko, Y. S., Ripke, S., Isaacs, A. & van Duijn, C. M. GenABEL: an R library for genome-wide association analysis. *Bioinformatics* **23**, 1294–1296 (2007).
30. MacArthur, J. et al. The new NHGRI-EBI Catalog of published genome-wide association studies (GWAS Catalog). *Nucleic Acids Res.* **45**, D896–D901 (2017).
31. Yang, J., Lee, S. H., Goddard, M. E. & Visscher, P. M. GCTA: atool for genome-wide complex trait analysis. *Am. J. Hum. Genet.* **88**, 76–82 (2011).
32. Pers, T. H. et al. Biological interpretation of genome-wide association studies using predicted gene functions.*Nat. Commun.* **6**, 5890 (2015).
33. Carithers, L. J. & Moore, H. M. The Genotype-Tissue Expression (GTEx) project. *Biopreserv. Biobank.* **13**, 307–308 (2015).
34. Ferreira, M. A. et al. Shared genetic origin of asthma, hay fever and eczema elucidates allergic disease biology. *Nat. Genet.* **49**, 1752–1757 (2017).
35. Durinck, S. et al. BioMart and Bioconductor: a powerful link between biological databases and microarray data analysis. *Bioinformatics* **21**, 3439–3440 (2005).
36. Bulik-Sullivan, B. et al. LD score regression distinguishes confounding from polygenicity in genome-wide association studies. *Nat. Genet.* **47**, 291–295 (2015).
37. Bulik-Sullivan, B. et al. An atlas of genetic correlations across human diseases and traits. *Nat. Genet.* **47**, 1236–1241 (2015).
38. Nagano, H. et al. p53-inducible DPYSL4 associates with mitochondrial supercomplexes and regulates energy metabolism in adipocytes and cancer cells. *Proc. Natl Acad. Sci. USA* **115**, 8370–8375 (2018).
39. Nauli, S. M. et al. Polycystins 1 and 2 mediate mechanosensation in the primary cilium of kidney cells. *Nat. Genet.* **33**, 129–137 (2003).
40. Bodle, J. C. et al. Primary cilia: the chemical antenna regulating human adipose-derived stem cell osteogenesis. *PLoS One* **8**, e62554 (2013).
41. Ahsan, M. et al. The relative contribution of DNA methylation and genetic variants on protein biomarkers for human diseases. *PLoS Genet.* **13**, e1007005 (2017).
42. Berkson, J. Limitations of the application of fourfold table analysis to hospital data. *Biometrics Bull.* **2**, 47–53 (1946).
43. Bowden, J., Davey Smith, G., Haycock, P. C. & Burgess, S. Consistent estimation in Mendelian randomization with some invalid instruments using a weighted median estimator. *Genet. Epidemiol.* **40**, 304–314 (2016).
44. Bowden, J., Smith, G. D. & Burgess, S. Mendelian randomization with invalid instruments: effect estimation and bias detection through Egger regression. *Int. J. Epidemiol.* **44**, 512–525 (2015).

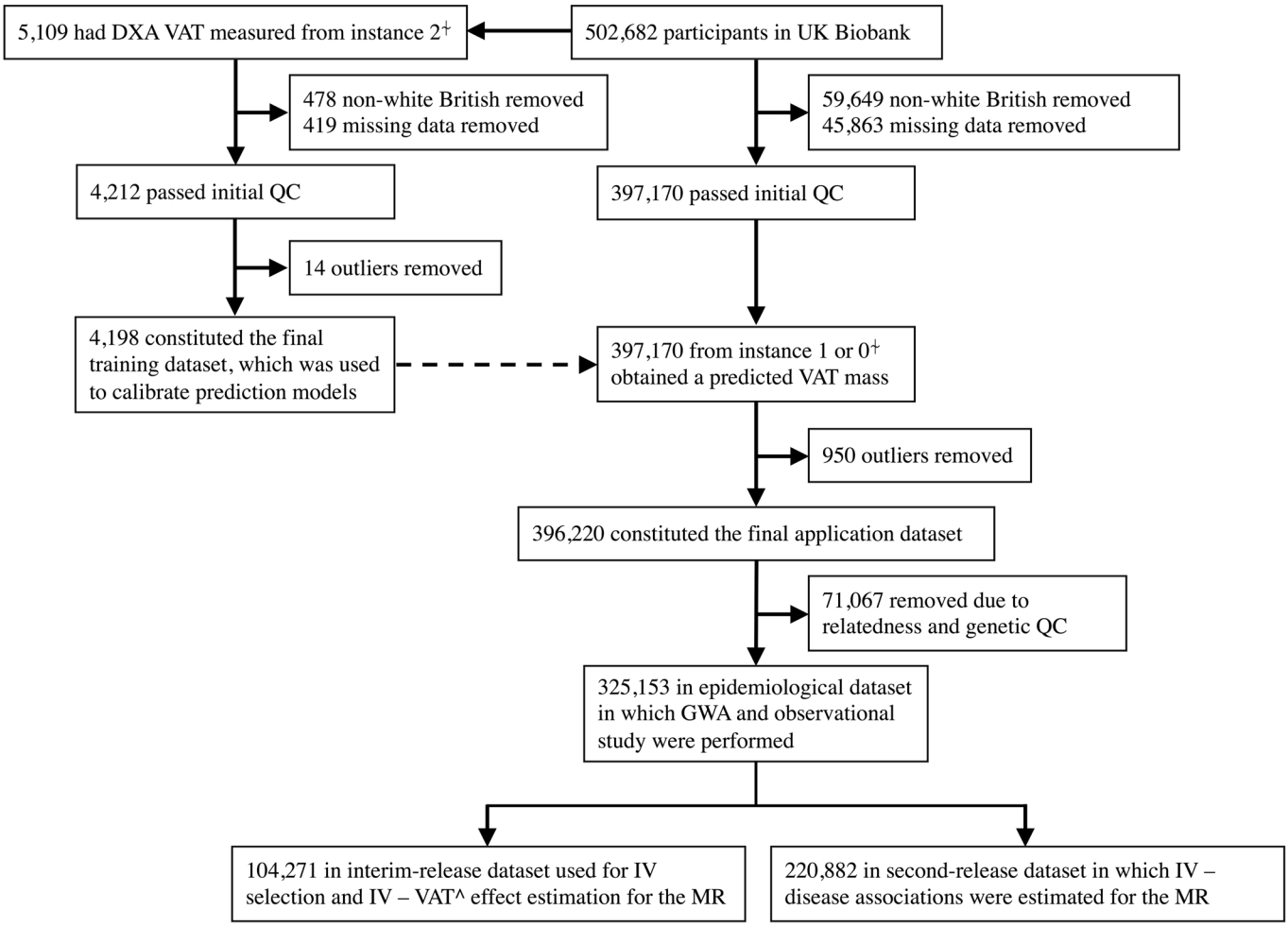

Extended Data Fig. 1 | Study selection. Instances 0, 1 and 2 denote different data collection time periods (instance 0, 2006–2010; instance 1, 2012–2013; instance 2, 2014 to the present). At instance 2, VAT mass was measured by DXA. For the MR analysis, the cohort was split into two nonoverlapping subsets. IV, instrumental variable.

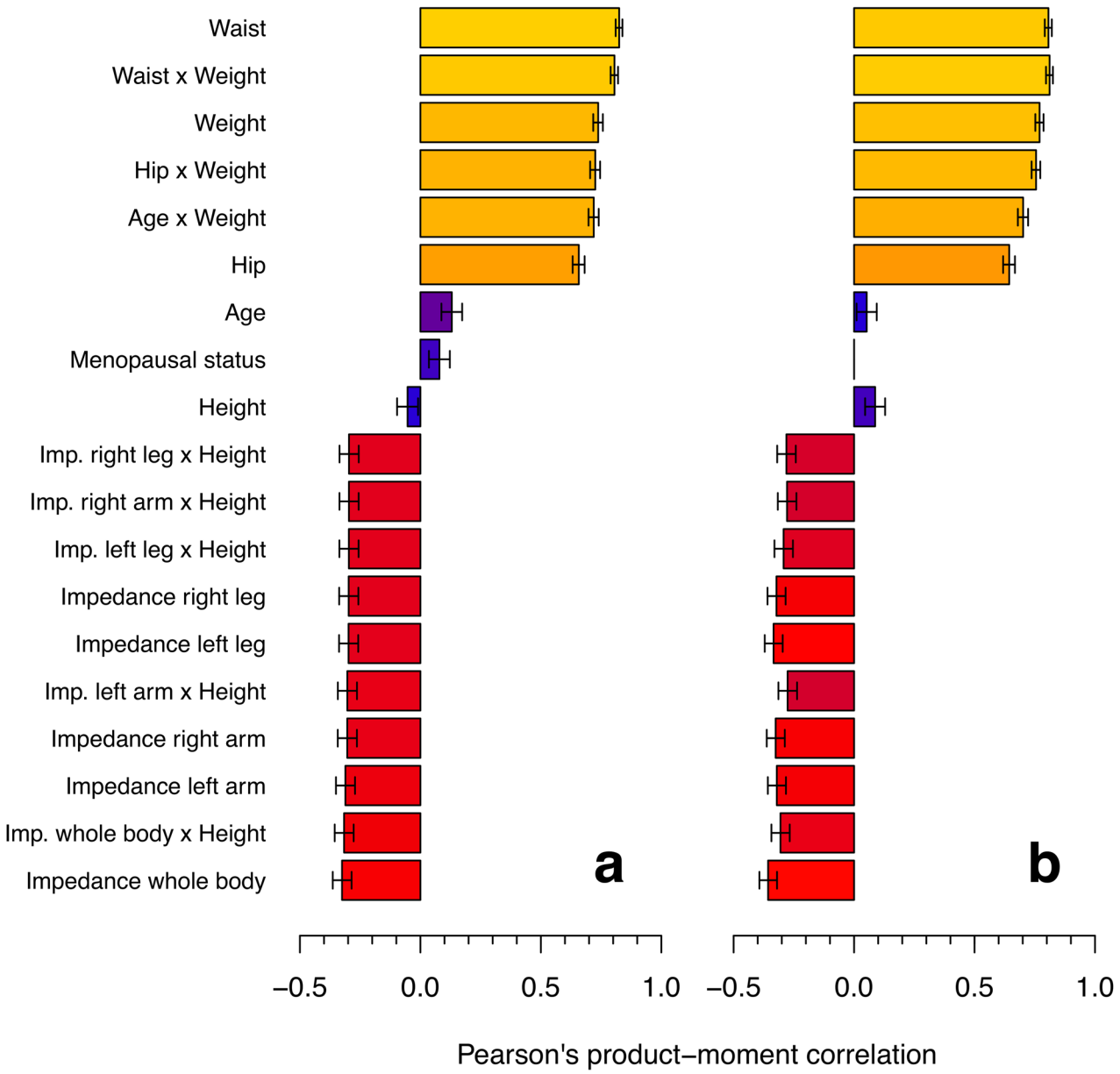

Extended Data Fig. 2 | Correlations between predictors and measured VAT mass. a,**b**, The length of each bar denotes the strength of the pairwise Pearson's product-moment correlation between the regression predictor (specified on the left) and measured VAT mass, for the female (**a**) and male (**b**) training datasets. The strength of the correlation is also visualized by color (dark blue, lowest correlation; yellow, highest correlation). The regression predictors are ordered from largest positive to largest negative correlation in females. Error bars denote 95% asymptotic CIs based on Fisher's *Z* transform. Sample sizes are $n = 2{,}010$ for females and $n = 2{,}188$ for males.

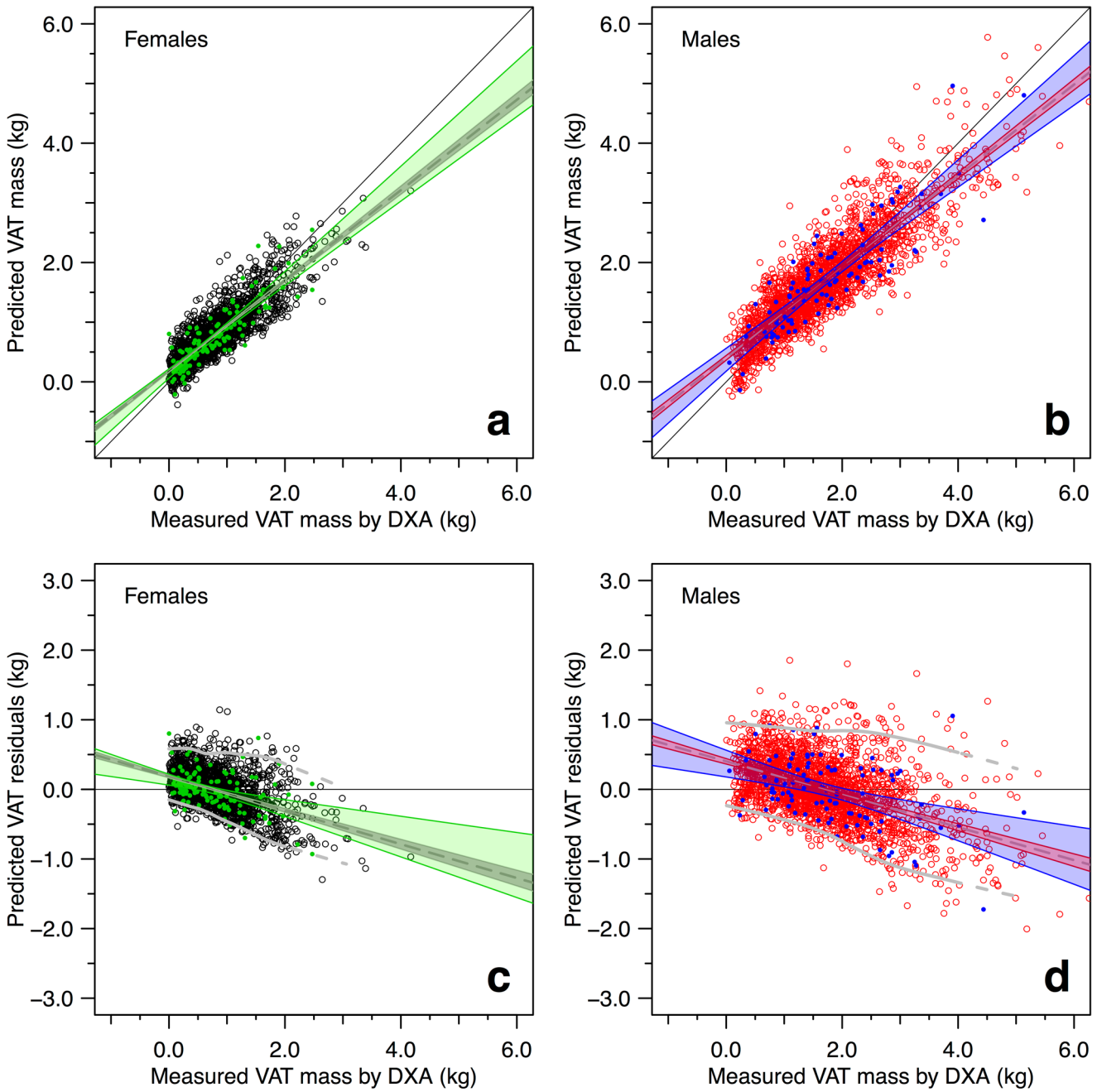

Extended Data Fig. 3 | Bias and 95% CIs of full prediction models, as a function of measured VAT. **a**,**b**, VAT^, as predicted from the leave-one-out cross-validation, plotted against measured VAT mass for females (**a**; black circles) and males (**b**; red circles). Also plotted is VAT^ against measured VAT mass for the out-of-sample data (green dots in **a** and blue dots in **b**). The out-of-sample datasets constitute Irish and other white individuals from the UKBB, excluding white British. The sample sizes are $n = 2{,}010$ females and $n = 2{,}188$ males for the training datasets, and $n = 119$ females and $n = 102$ males for the out-of-sample datasets. The long-dashed, gray lines denote the linear fits (ordinary least squares regression) to the leave-one-out cross-validation data, and the gray (**a**) and red shaded areas (**b**) denote the corresponding CIs of the estimated slopes. Green (**a**) and blue shaded areas (**b**) denote the CIs of the linear fits (not plotted) to the out-of-sample data. Thin black lines denote the one-to-one relation. A slope below the one-to-one relation indicates that a small bias is present in the data. However, note that the attenuation is exaggerated due to measurement errors also in the measured VAT mass. **c**,**d**, VAT prediction residuals plotted against measured VAT mass for females (**c**) and males (**d**). The long-dashed lines correspond to the fitted regression lines in **a** and **b**. The gray, solid lines denote the conditional 95% CIs. These lines become dashed at high VAT mass, to indicate an increasing uncertainty in the CIs. Otherwise, symbols are as in **a** and **b**.

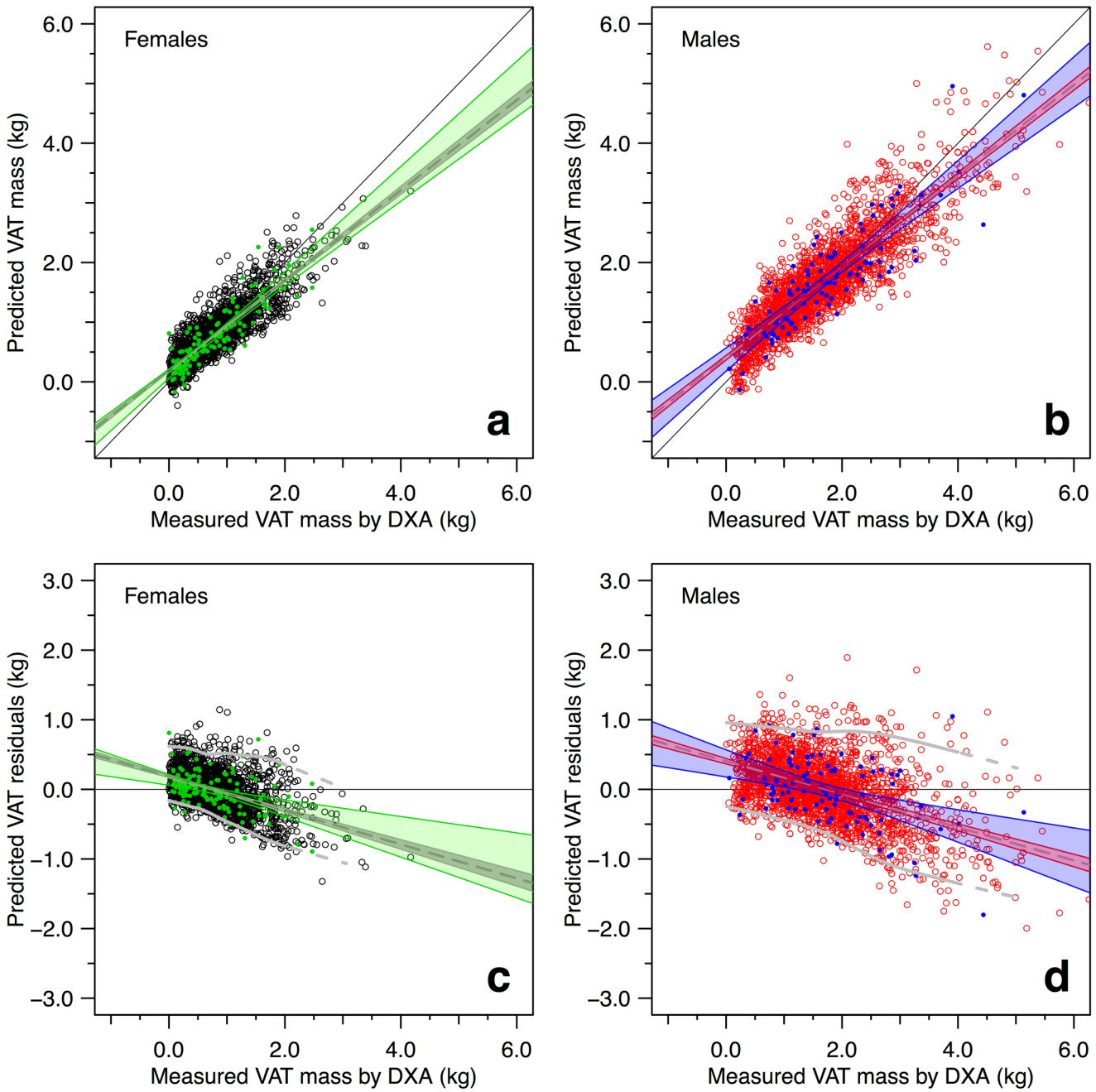

Extended Data Fig. 4 | Bias and 95% CIs of reduced prediction models, as a function of measured VAT. Symbols and sample sizes as in Extended Data Fig. 3.

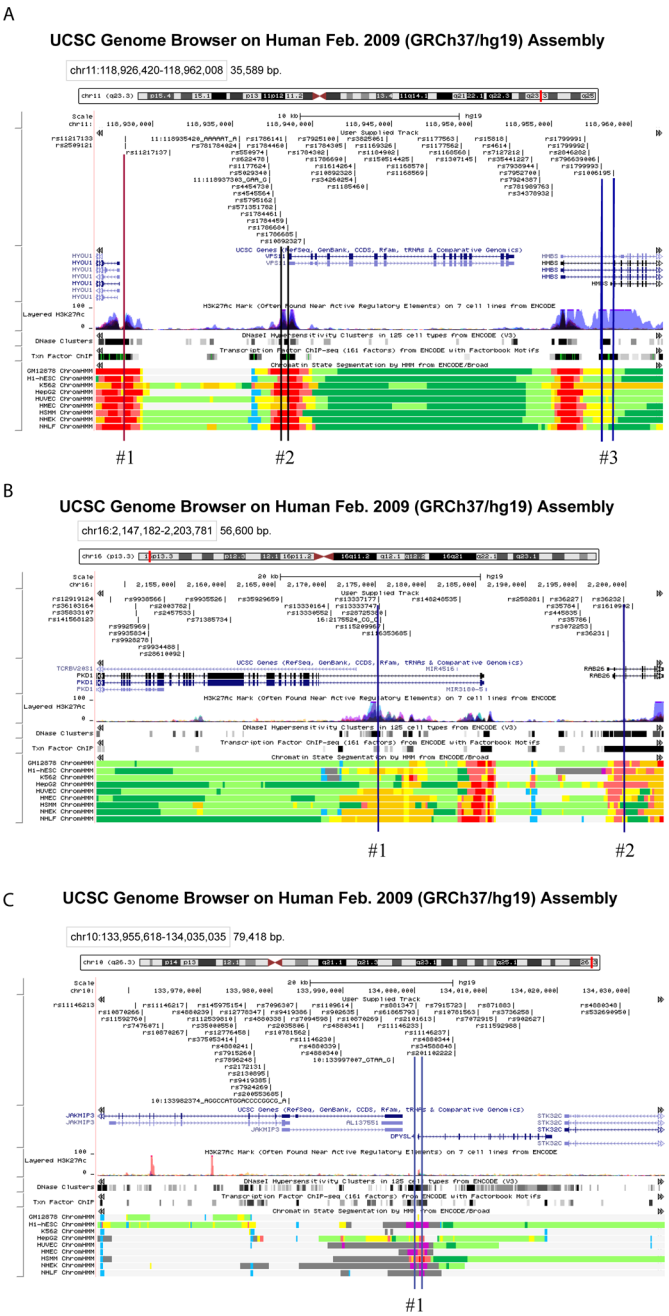

Extended Data Fig. 5 | Overview of the genomic locations of the selected SNPs in the functional study. The locations of the SNPs are indicated by vertical lines. **a**, The *HMBS/VPS11* region. Region 1 contains two SNPs (rs2509121 and rs11217133). Region 2 contains five SNPs (rs1784461, rs1786141, rs1784460, rs1784459 and rs1786684). Region 3 contains two SNPs (rs1799993 and rs1006195). **b**, The *PKD1* region. Region 1 contains one SNP (rs13337177). Region 2 contains one SNP (rs36232). **c**, The *DPYSL4* region. Region 1 contains three SNPs (rs881347, rs61865793 and rs11146233).

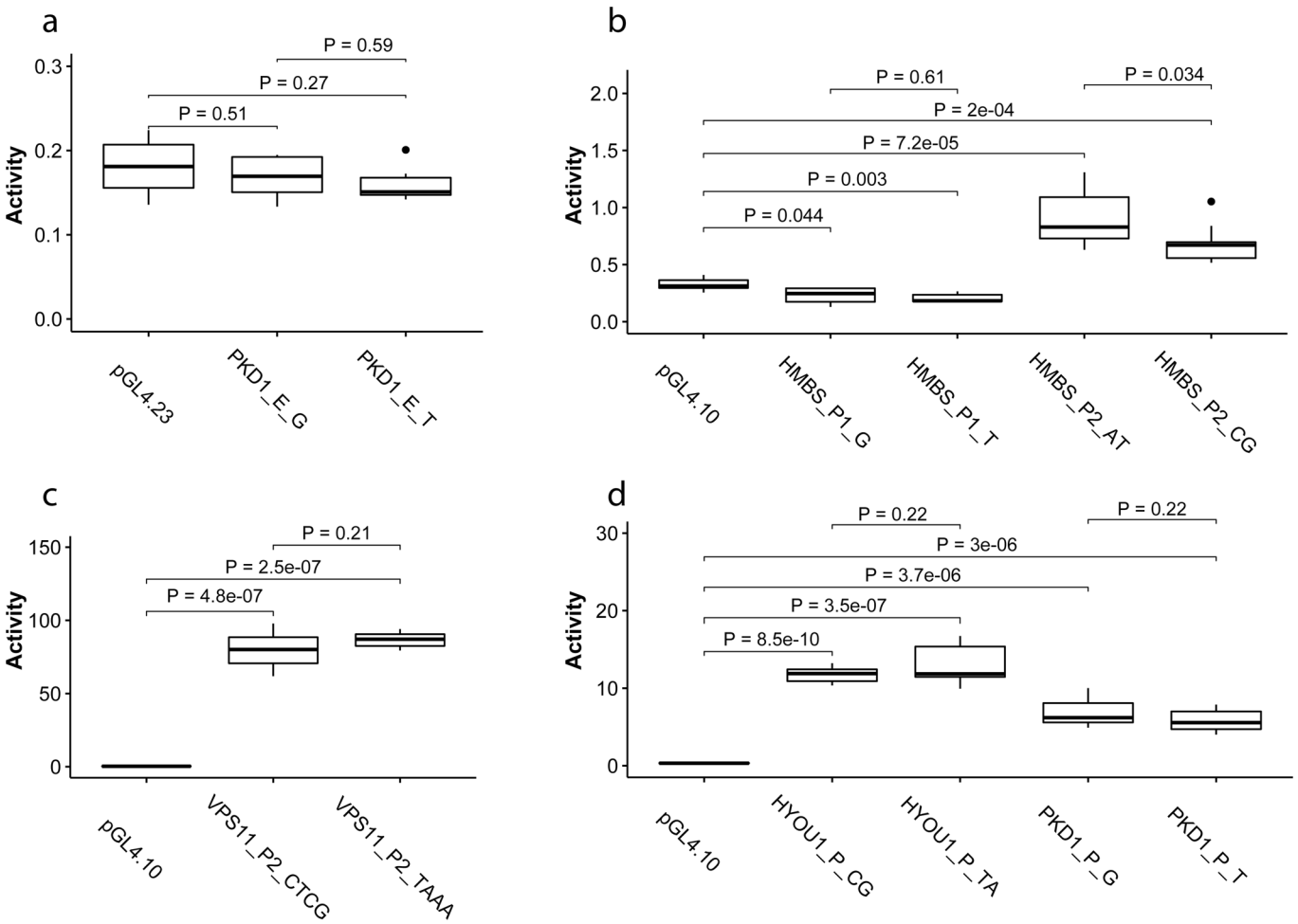

Extended Data Fig. 6 | Results from the luciferase assay in HepG2 cells. For each set of alleles, the box plots represent the median, interquartile range, and minimum and maximum values of all replicates, except for outliers, which are represented as individual points. The total number of replicates of each plasmid is given by the number of independent plasmid extractions multiplied by the number of independent transfections. The *P* values (two-sided *t*-test) represent pairwise differences in means, either for the control plasmid (pGL4.10 or pGL4.23) without any insert versus the same plasmid with one of the fragments inserted, or for the two plasmids with fragments, with different alleles inserted. In the names, the subscripts _E and _P indicate whether the fragment was cloned as an enhancer (_E) or promoter (_P) element, with _P1 and _P2 representing two different fragments in the same promoter region. The last part of the names represents the alleles of the SNPs that were targeted by each fragment (see Supplementary Table 14). Two to three independent plasmid extractions and transfections were performed, with each transfection being replicated three times.

	cases/controls	OR (95% CI)
Type 2 diabetes with:	**4 670/154 511**	**4.95 (4.74–5.17)**
coma	13/154 511	3.67 (2.14–6.31)
ketoacidosis	30/154 511	2.55 (1.59–4.09)
renal complications	26/154 511	6.10 (4.23–8.79)
ophthalmic compl.	187/154 511	4.92 (4.21–5.76)
neurological compl.	80/154 511	5.61 (4.48–7.03)
peripheral circul. compl.	30/154 511	6.32 (4.65–8.59)
no complications	4374/154 511	4.96 (4.74–5.19)

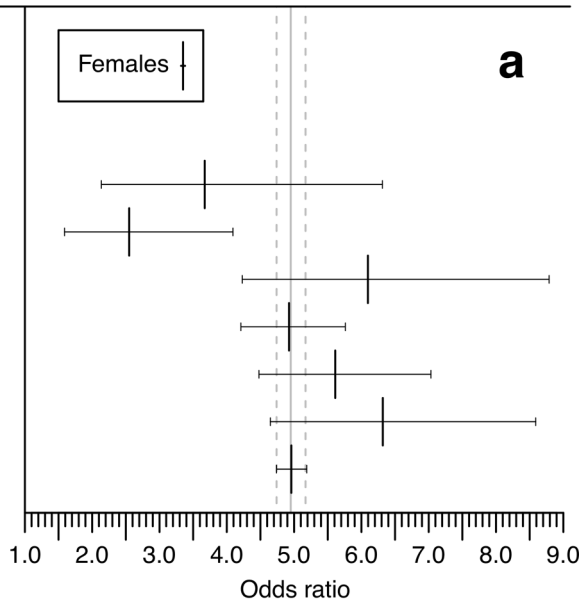

	cases/controls	OR (95% CI)
Type 2 diabetes with:	**10 002/150 830**	**2.43 (2.38–2.49)**
coma	42/150 830	2.43 (1.89–3.11)
ketoacidosis	42/150 830	1.65 (1.17–2.32)
renal complications	112/150 830	2.69 (2.30–3.16)
ophthalmic compl.	549/150 830	2.21 (2.04–2.40)
neurological compl.	256/150 830	2.81 (2.53–3.13)
peripheral circul. compl.	175/150 830	2.53 (2.22–2.89)
no complications	9357/150 830	2.45 (2.40–2.51)

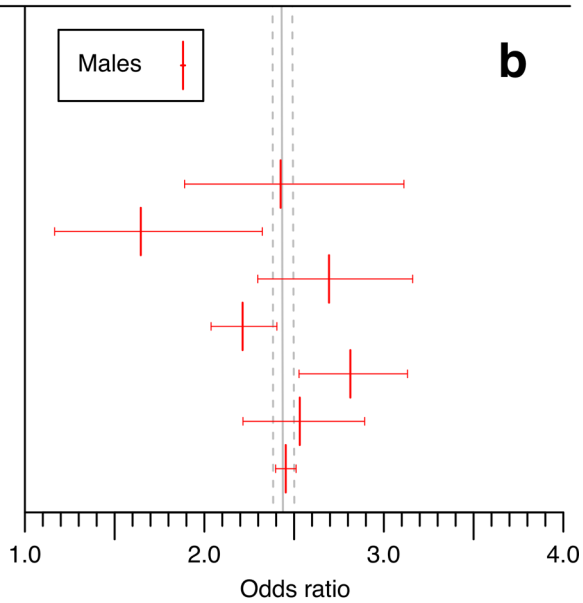

Extended Data Fig. 7 | Effect of VAT^ on the risk of developing type 2 diabetes for subgroups with specified medical complications. a,**b**, Estimated ORs for females (**a**) and males (**b**). The solid, gray lines and 95% CIs (dashed gray lines) correspond to the OR estimated for all female (**a**) or male cases (**b**) (see bold text to the left; see also Fig. 2). The black (**a**) and red vertical lines (**b**) (with error bars denoting 95% CIs) denote the ORs for the various subgroups with specific medical complications. Note the difference in scale between the two panels. All ORs refer to an increase of 1kg in VAT^.

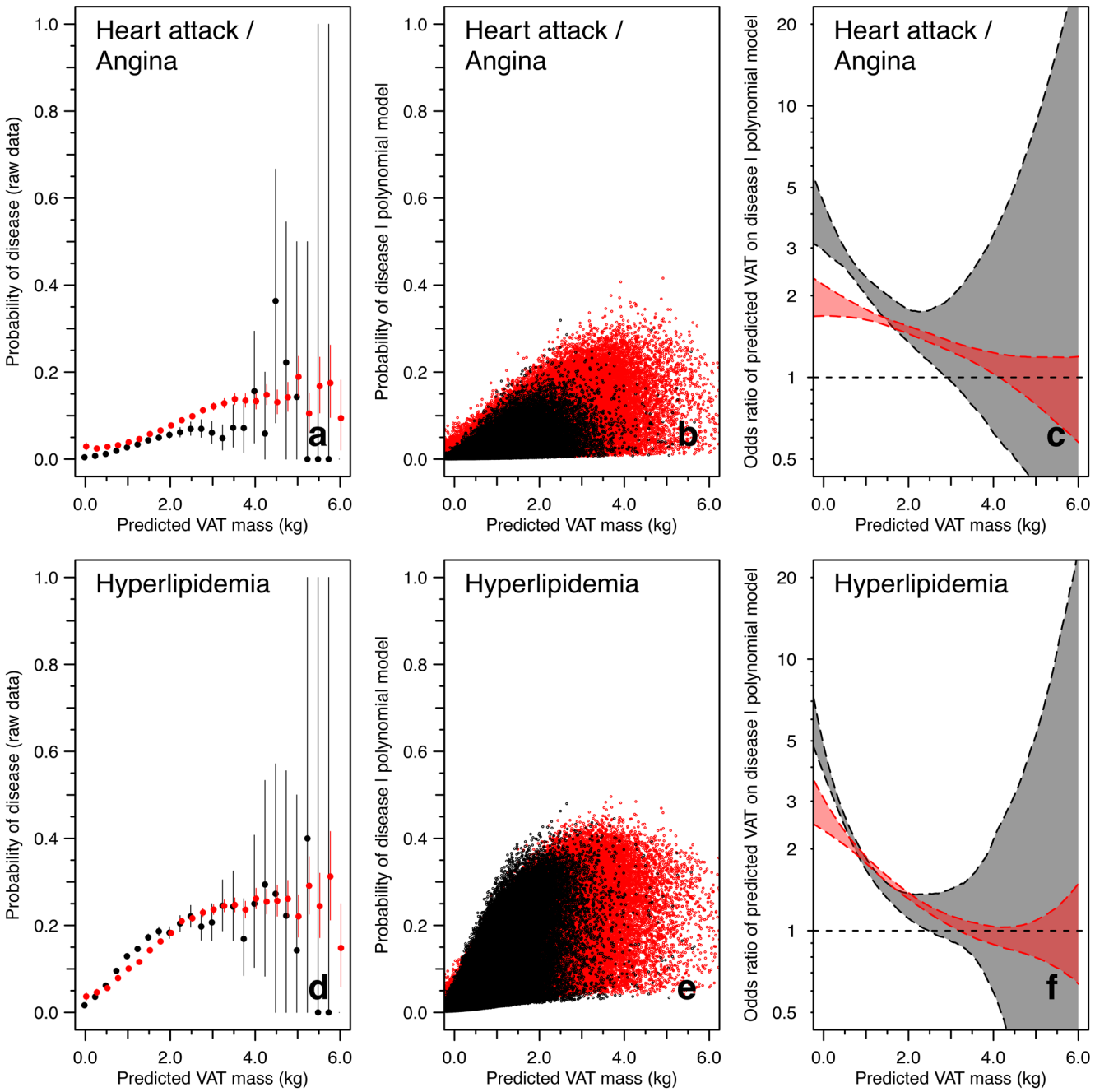

Extended Data Fig. 8 | Polynomial logistic regression models for heart attack/angina and hyperlipidemia. a–**f**, Models for heart attack/angina (**a**–**c**) and hyperlipidemia (**d**–**f**), showing the probability of disease for the raw, unadjusted data (**a** and **d**), the predicted probability of disease for each individual (**b** and **e**), given the adopted polynomial model (see Supplementary Table 17), and 95% (basic bootstrap) confidence bands (shaded areas) of the ORs per one-unit increase (1 kg) in VAT^ (**c** and **f**), each as a function of VAT^. In **a** and **d**, error bars indicate 95% CIs, based on the Poisson statistics. The total numbers of cases and controls for heart attack/angina and hyperlipidemia are given in Fig. 2 for females and males separately. In all panels, black and gray denote females while red and pink denote males.

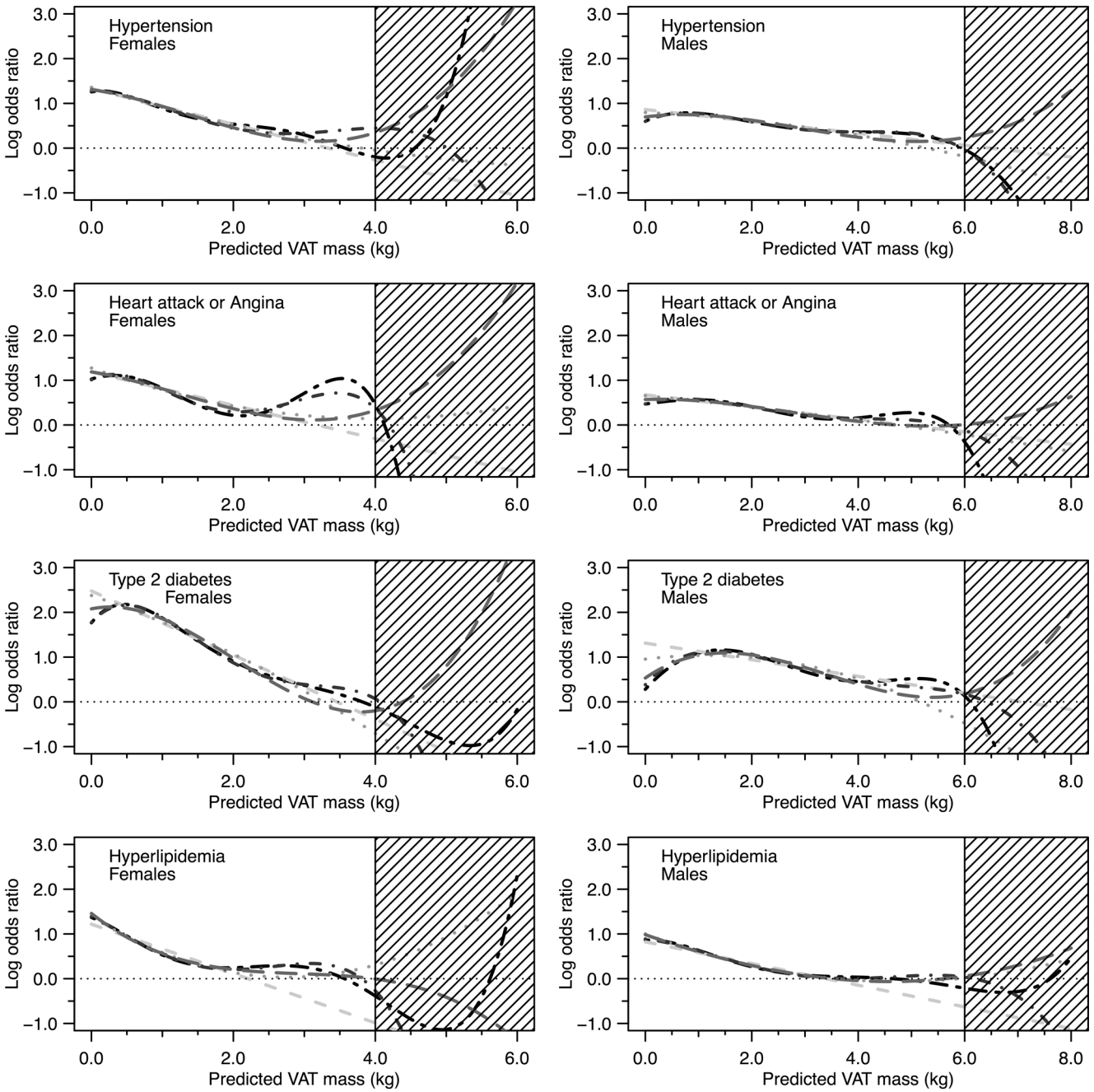

Extended Data Fig. 9 | Sensitivity test for the polynomial logistic regression models. Each panel shows the log[OR] for five different models that are polynomial in VAT^ to different degrees: dashed lines denote second-degree polynomials ($q=2$); dotted lines denote third-degree polynomials ($q=3$); long-dashed lines denote fourth-degree polynomials ($q=4$); dot-dashed lines denote fifth-degree polynomials ($q=5$); and two-dashed lines denote sixth-degree polynomials ($q=6$). The lines are also color-coded from light gray ($q=2$) to black ($q=6$). All models also include age, smoking behavior and 15 principal components as covariates. The models are polynomial in age, with degrees of the polynomials as indicated in Supplementary Table 17. Shaded areas indicate regions of large model uncertainty. Note that for each disease, all models show a very similar functional form of the log[OR], independent of the degree of the polynomial.

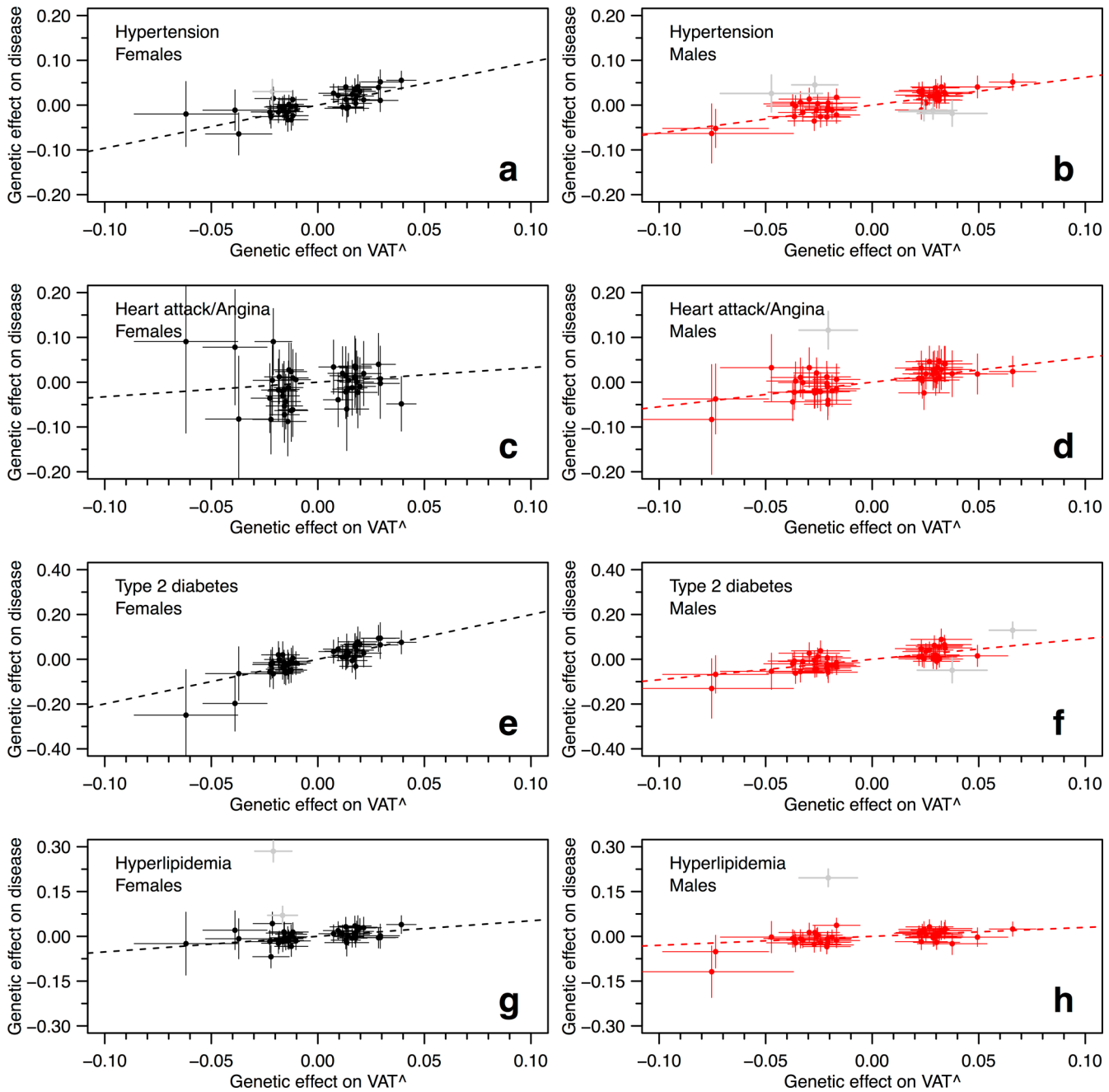

Extended Data Fig. 10 | Relationship between the effects of the genetic instruments on VAT^ and their effects on disease. Each panel shows the relationship between the effects on VAT^ and the effects on disease of the $n = 44$ nearly independent genetic instruments (Supplementary Table 21). Error bars denote the 95% CI (normal approximation) of each effect estimate. Females are denoted in black, while males are denoted in red. Pleiotropic outliers identified by the GSMR analysis that were removed before estimation of the causal effects are shown in gray (Supplementary Table 22). An observed slope is indicative of a causal relationship between VAT^ and disease that is unbiased by confounding. The dashed lines denote the estimated log[OR] values by the gsmr package (Table 1). Note the different scales of the *y* axes.

nature research

Corresponding author(s): Torgny Karlsson & Åsa Johansson

Last updated by author(s): July 22, 2019

Reporting Summary

Nature Research wishes to improve the reproducibility of the work that we publish. This form provides structure for consistency and transparency in reporting. For further information on Nature Research policies, see Authors & Referees and the Editorial Policy Checklist.

Statistics

For all statistical analyses, confirm that the following items are present in the figure legend, table legend, main text, or Methods section.

n/a	Confirmed	
☐	☒	The exact sample size (*n*) for each experimental group/condition, given as a discrete number and unit of measurement
☐	☒	A statement on whether measurements were taken from distinct samples or whether the same sample was measured repeatedly
☐	☒	The statistical test(s) used AND whether they are one- or two-sided *Only common tests should be described solely by name; describe more complex techniques in the Methods section.*
☐	☒	A description of all covariates tested
☐	☒	A description of any assumptions or corrections, such as tests of normality and adjustment for multiple comparisons
☐	☒	A full description of the statistical parameters including central tendency (e.g. means) or other basic estimates (e.g. regression coefficient) AND variation (e.g. standard deviation) or associated estimates of uncertainty (e.g. confidence intervals)
☐	☒	For null hypothesis testing, the test statistic (e.g. *F*, *t*, *r*) with confidence intervals, effect sizes, degrees of freedom and *P* value noted *Give P values as exact values whenever suitable.*
☒	☐	For Bayesian analysis, information on the choice of priors and Markov chain Monte Carlo settings
☒	☐	For hierarchical and complex designs, identification of the appropriate level for tests and full reporting of outcomes
☐	☒	Estimates of effect sizes (e.g. Cohen's *d*, Pearson's *r*), indicating how they were calculated

Our web collection on statistics for biologists contains articles on many of the points above.

Software and code

Policy information about availability of computer code

Data collection	No specific software or computer codes were used by us to collect data. Data were directly downloaded from the UK Biobank Resource.
Data analysis	R version 3.4.2 including lm (stats v3.5.3), glm (stats v3.5.3), rms (v5.1-2), simex (v1.7), polyroot (base v3.6.1), biomaRt (v2.34.2), gsmr (v.1.0.7), MendelianRandomization (v0.4.1), and GenABEL(1.8-0); PLINK v1.90b3n; GCTA v1.26.0; ldsc v1.0.0; GTEx v7; DEPICT v1.1.

For manuscripts utilizing custom algorithms or software that are central to the research but not yet described in published literature, software must be made available to editors/reviewers. We strongly encourage code deposition in a community repository (e.g. GitHub). See the Nature Research guidelines for submitting code & software for further information.

Data

Policy information about availability of data

All manuscripts must include a data availability statement. This statement should provide the following information, where applicable:

- Accession codes, unique identifiers, or web links for publicly available datasets
- A list of figures that have associated raw data
- A description of any restrictions on data availability

This research was conducted using the UK Biobank Resource under Application Number 15152, following the restrictions on data availability as decided by the UK Biobank.

Field-specific reporting

Please select the one below that is the best fit for your research. If you are not sure, read the appropriate sections before making your selection.

☒ Life sciences ☐ Behavioural & social sciences ☐ Ecological, evolutionary & environmental sciences

For a reference copy of the document with all sections, see nature.com/documents/nr-reporting-summary-flat.pdf

Life sciences study design

All studies must disclose on these points even when the disclosure is negative.

Sample size	The UK Biobank is a publicly available population-based cohort. No sample-size calculations were performed prior to data analysis, the sample size was chosen based on the sample size in the publicly available dataset.
Data exclusions	Data exclusion/filtering was performed both on phenotypic and genotypic level. Only white British participants were included in the analyses, to avoid bias or/and variance inflation due to population structure. Individuals who answered "do not know", "prefer not to answer", or had missing entries in any of the explored predictor variables or in the response (measured VAT mass by DXA) were removed. In addition, a number of extreme outliers were removed in the predictor variables, such as all individuals who had changed their body-mass index (BMI) more than eight units between instance 0 or 1 and the instance at which VAT was measured (i.e., instance 2), individuals with inadequate menopausal status, and individuals with extremely low waist circumference (<= 26 cm) but otherwise with average body size measures. Furthermore, a number of individuals with extreme hip circumference in relation to their BMI were removed. Also, all individuals with a difference in impedance between left and right arm or left and right leg of >120 ohm were removed as were extreme impedance measures in relation to the individual's BMI. These criteria were applied both to the training data set and the application data set and only eleven individuals with an extreme predicted VAT mass had to be removed before the logistic regression and the genome-wide association (GWA) study were performed. At the genotypic level, an additional filtering was performed including only participants classified as Caucasians by principal component analysis. Individuals were also excluded due to relatedness based on kinship data (estimated genetic relationship >0.044) and individuals with poor call rate (<95%), with high heterozygosity or with sex-errors were removed. The exclusion criteria on the genotypic level were established prior to the study. Finally, SNPs were filtered based on call rate (>99%), deviance from Hardy-Weinberg equilibrium (HWE) such that p>1E-20, minor allele frequency (MAF) such that MAF>0.001 and imputation quality (>0.3).
Replication	Out-of-sample validation was used to validate the performance of the prediction models and to verify that over-fitting was not an issue. In line with the cross validation and the bootstrapping, out-of-sample validation was successful and the models were not over-fitted. As regards the GWA study, no replication was performed, but a family-wise error rate of alpha<0.05 was ensured by adopting a p-value threshold of p=3.33E-09 for genome-wide significance, in order not to have an inflated type I error.
Randomization	A subset of the UK biobank participants were invited to the imaging study that produced the DXA scan variables that has been used to estimate visceral fat mass. This subset of participants was selected independently from the information that had previously been collected but was biased towards participants living within a reasonable traveling distance to one of the imaging assessment centers.
Blinding	Doctors and nurses were not blinded to individual participants during e.g., verbal interviews. However, prior to data and laboratory analyses all data and samples were anonymized.

Reporting for specific materials, systems and methods

We require information from authors about some types of materials, experimental systems and methods used in many studies. Here, indicate whether each material, system or method listed is relevant to your study. If you are not sure if a list item applies to your research, read the appropriate section before selecting a response.

Materials & experimental systems

n/a	Involved in the study
☒	☐ Antibodies
☐	☒ Eukaryotic cell lines
☒	☐ Palaeontology
☒	☐ Animals and other organisms
☐	☒ Human research participants
☒	☐ Clinical data

Methods

n/a	Involved in the study
☒	☐ ChIP-seq
☒	☐ Flow cytometry
☒	☐ MRI-based neuroimaging

Eukaryotic cell lines

Policy information about cell lines

Cell line source(s)	We used the HepG2 cell line, purchased from ATCC (ATCC Number HB-8065).
Authentication	The cell line was authenticated by ATCC at purchase.

Mycoplasma contamination	The cells were tested negative for Mycoplasma contamination.
Commonly misidentified lines (See ICLAC register)	No misidentified cell line was used.

Human research participants

Policy information about studies involving human research participants

Population characteristics	The UK Biobank is a very large and detailed prospective study with over 500,000 participants (both females and males) aged 40-69 years at the time of recruitment in 2006-2010.
Recruitment	The UK Biobank database includes 502,682 participants recruited from all across the UK. Participants were recruited between 2006 and 2010. Most participants visited the center once, but some individuals visited the center at up to three instances. Selection bias, potentially affecting the non-linear results presented in this study, may arise if diseased individuals with high depots of visceral fat opted-out from participating in the study to a higher degree as compared to diseased individuals with lower depots of visceral fat. That said, the fact that all estimated odds ratios appear to approach unity would be contrived from the point of view of selection bias, since a detailed balance between an increase in visceral fat and an increase in the fraction of diseased individuals opting-out from participation must, in that case, be maintained.
Ethics oversight	Ethical approval was given to the UKBB resource by the North West Multicentre Research Ethics Committee (covering the UK), the National Information Governance Board for Health & Social Care (covering England and Wales), and the Community Health Index Advisory Group (covering Scotland). UKBB possesses a generic Research Tissue Bank approval granted by the National Research Ethics Service, which lets applicants conduct research on UKBB data without obtaining separate ethical approvals. Written consent was obtained from all UKBB participants.

Note that full information on the approval of the study protocol must also be provided in the manuscript.